Materials Advances

ROYAL SOCIETY OF CHEMISTRY

PAPER

View Article Online
View Journal | View Issue

Check for updates

Cite this: *Mater. Adv.*, 2025, 6, 1769

Novel biocompatible multifunctional porous magnetic nanoclusters for the targeted delivery of lenvatinib towards hepatocellular carcinoma†

Saba Sohail,[ab] Alam Zeb,[c] Ali H. Alamri,[d] Adel Al Fatease,[d] Ahmed A. Lahiq,[e] Nabil K. Alruwaili,[f] Salman Khan[a] and Fakhar ud Din *[ab]

Hepatocellular carcinoma (HCC) is a very aggressive and deadly disease with a complicated tumor microenvironment (TME). Recently, lenvatinib (LEN) has shown effectiveness in the clinical treatment of HCC, but its limited solubility and serious adverse reactions must not be overlooked. Herein, we developed novel pluronic F127-decorated citric acid-capped, LEN-loaded porous magnetic nanoclusters (PF127/CA/LEN@pMNCs) for effective tumor targeting and toxicity reduction. PF127/CA/LEN@pMNCs were statistically optimized and characterized based on their particle size, polydispersity index (PDI), zeta potential, and entrapment efficiency (%EE). Additionally, Fourier transform infrared (FTIR) spectroscopy, scanning electron microscopy (SEM), transmission electron microscopy (TEM), differential scanning calorimetry (DSC), and X-ray diffraction (XRD) analyses were performed. Furthermore, advanced characterization techniques such as vibrating sample magnetometry (VSM), Brunauer–Emmett–Teller (BET) method, thermal gravimetric analysis (TGA) and inductively coupled plasma-optical emission spectroscopy (ICP-OES) were employed. In addition to these, *in vitro* release, hemolytic assay, lactate dehydrogenase (LDH) assay, cell viability and magnetic hyperthermia (MH) analyses of PF127/CA/LEN@pMNCs were performed. Cytotoxicity assay of PF127/CA/LEN@pMNCs under magnetic hyperthermia (MH) exposure conditions was also performed using H22 and Hep3B cells. The successful production of PF127/CA/LEN@pMNCs was confirmed by FTIR spectroscopy and TGA analysis. The optimized PF127/CA/LEN@pMNCs demonstrated 160 nm particle size, −22.80 mV zeta potential, 98% EE, 8.9% loading capacity, hemocompatibility, superparamagnetism, and a prolonged retention time. The iron content of nanoclusters was found to be between 55.78% and 83.91%. Moreover, PF127/CA/LEN@pMNCs exhibited pH responsiveness, and they significantly ($p < 0.05$) reduced the cell viability of H22 and Hep3B cells. The specific absorption rate of PF127/CA/LEN@pMNCs was 10.79 W g^{-1} at 10 mg mL^{-1}, indicating their potential for MH. Additionally, significantly ($p < 0.05$) improved cytotoxicity of PF127/CA/LEN@pMNCs was confirmed against H22 and Hep3B cells under the influence of MH. Collectively, this novel research offers valuable insights into harnessing the diverse potentials of combining existing pharmaceuticals with metallic nanomedicine to effectively treat the intractable liver cancer.

Received 5th November 2024,
Accepted 2nd February 2025

DOI: 10.1039/d4ma01101e

rsc.li/materials-advances

1 Introduction

The annual morbidity rate of HCC has been reported to be 10 cases per 100 000 individuals globally.[1] HCC is currently ranked as the third most prevalent malicious tumor globally,[2] and it is expected to become the 2nd highest cause of cancer-associated mortality.[3,4] It usually exhibits obscure early stages, high recurrence rate, and metastasis after surgery.[5] Therapeutic approaches for initial-stage liver cancer comprise liver transplantation, surgical excision, and interventional therapy.[6] However, a majority of clinical cases are typically identified when the tumor has already reached an advanced stage, making it impossible to effectively treat with surgery and thereby requiring chemotherapy.[7] In 2018,

[a] *Department of Pharmacy, Quaid-i-Azam University, Islamabad 45320, Pakistan. E-mail: fudin@qau.edu.pk*
[b] *Nanomedicine Research Group, Department of Pharmacy, Quaid-i-Azam University, Islamabad, Pakistan*
[c] *College of Pharmacy, Hanyang University, Ansan 15588, South Korea*
[d] *Department of Pharmaceutics, College of Pharmacy, King Khalid University, Abha 62529, Saudi Arabia*
[e] *Department of Pharmaceutics, College of Pharmacy, Najran University, Najran 66262, Saudi Arabia*
[f] *Pharmaceutics Department, College of pharmacy, Jouf University, Sakaka, Saudi Arabia*

† Electronic supplementary information (ESI) available. See DOI: https://doi.org/10.1039/d4ma01101e

the FDA approved lenvatinib (LEN) for the treatment of progressive HCC.[8] LEN hinders the activity of receptor tyrosine kinases (RTKs), which comprise platelet-attained growth factor receptor-α/β (PDGFR-α/β); fibroblast growth factor receptor (FGFR) 1, 2, 3, and 4; KIT; and RET. LEN exhibits selective direct antiproliferative effects in hepatic cell lines (Hep 3B) depending upon active FGFR signaling.[9] Moreover, it demonstrates efficacy in H22 cells,[10] although the level of sensitivity varies owing to the inherent variations between the cell lines. A graphical illustration is given in Fig. S1 (ESI†).[11] Despite the proven effectiveness of LEN in cancer treatment, its limited aqueous solubility (less than 1 mg mL^{-1}), pharmacokinetics, and undesirable side effects, including, joint pain, weight loss, fatigue, hypertension, and diarrhea, limit its widespread application in HCC patients.[12] These limitations often lead to a low level of patient acceptance and adherence, thus hampering the broad therapeutic applicability of LEN.[13] Given the drawbacks, it is imperative to research the utilization of multifunctional drug delivery vehicles and combination therapy to overcome these limitations. Significant advancements in nanotechnology have successfully addressed the issues related to drug carriers, leading to substantial improvements in chemotherapy.[14,15]

Porous magnetic nanoclusters (pMNCs) are the multifunctional platforms among various NPs that can assist as drug carriers in HCC.[16] Moreover, magnetic nanoparticles (MNPs) hold significant ability as theranostic agents with a widely recognized profile and FDA authorization for human use in the biomedical field.[17] They allow the release of the drug at a precise rate and site,[18] thereby leading to the targeted distribution of antitumor drugs, hyperthermia therapy (HT), and monitoring of the effectiveness of therapy using imaging-guided treatments.[17] Recent findings have verified that the clustering of MNPs exhibited much higher values of saturation magnetization (M_s) and specific absorption rate (SAR) than those of individual MNPs.[19] The effectiveness of these particles relies on their magnetism, dispersion, biocompatibility, and degree of aggregation. The last two factors, in particular, pose challenges and restrict the use of MNPs in biological settings.[20]

To tackle these problems, it is conceivable to apply a layer of capping agents and a biocompatible polymer to the MNPs, therefore enhancing both the biodegradability and stability of the particles.[20] To achieve this objective, citric acid (CA), a substance with a high electric charge, is a suitable choice for coating particles, particularly MNPs that exhibit a robust magnetic interaction.[18] CA displays great biocompatibility and presents both electrostatic and steric repulsion properties.[21] Moreover, to further stabilize the MNPs in magnetic diagnostic techniques such as magnetic resonance imaging (MRI) and magnetic hyperthermia (MH), a coating of pluronic F127 (PF127) was applied.[18] Moreover, the encapsulation of MNPs using PF127 may enhance their stability in an aqueous environment.[4]

This research aimed to design novel PF127/CA/LEN@pMNCs for potential targeting of HCC. The PF127/CA/LEN@pMNCs were optimized using the statistical design software Design-Expert®. The first layer contained porous Fe_3O_4 deposited *via* a one-step coprecipitation method that incorporated LEN in the presence of a low-molecular-weight binding agent, polyacrylic acid (PAA). CA capped the second layer as a stabilizing agent and an electrostatic stabilizer. The third layer was finally decorated with PF127 to avoid aggregation and identification by the reticuloendothelial system (RES). The performance and physical attributes of PF127/CA/LEN@pMNCs were characterized by dynamic light scattering (DLS), scanning electron microscopy (SEM), transmission electron microscopy (TEM), Fourier transform infrared (FTIR) spectroscopy, differential scanning calorimetry (DSC), X-ray diffraction (XRD), vibrating sample magnetometry (VSM), Brunauer–Emmett–Teller (BET), thermogravimetric analysis (TGA) and inductively coupled plasma-optical emission spectroscopy (ICP-OES). Moreover, the optimized formulation was examined for *in vitro* release and anticancer properties against HCC cell lines (Hep3B and H22) followed by confirmation by a lactate dehydrogenase (LDH) assay. Moreover, a hemolysis test was performed followed by cytotoxicity analysis under MH conditions. To the best of our information, no pMNC system of LEN coated with CA and PF127 has been reported for targeting HCC so far, which makes this work novel.

2 Materials and methods

2.1 Materials

Ferric chloride hexahydrate ($FeCl_3{\cdot}6H_2O$), ferrous sulfate heptahydrate ($FeSO_4{\cdot}7H_2O$), and CA ($C_6H_8O_7$) were bought from Duksan (Ansan, South Korea) with a minimum purity of 99%. PAA was acquired from Macklin (Shanghai, China). NH_4OH (32%) with a minimum purity of 98%, dimethyl sulfoxide (DMSO), sodium chloride, sodium hydroxide, Tween® 80, PF127, and disodium hydrogen phosphate were acquired from Sigma Aldrich (Darmstadt, Germany). LEN was bought from Beijing Cooperate Pharmaceutical (Beijing, China). Neodymium magnets (NdFeB permanent magnets) were purchased from the local market. 3-(4,5-Dimethyl thiazol-2-yl)-2,5-diphenyltetrazolium bromide (MTT) was provided by Sigma-Aldrich (St. Louis, MO, USA). The other chemicals utilized in various studies were of analytical grade.

2.1.1 Cell lines. The liver cancer cell lines were procured from the Cell Bank of the Type Culture Collection of the Chinese Academy of Sciences (Shanghai, China). H22 and Hep3B cells were incubated in an incubator at a temperature of 37 °C at a carbon dioxide concentration of 5%. The H22 medium comprised RPMI 1640 supplemented with 10% fetal bovine serum (FBS), while the Hep3B media was Dulbecco's modified Eagle's medium (DMEM) (Gibco) supplemented with 10% FBS, 100 international units per milliliter of penicillin as well as 100 micrograms per milliliter of streptomycin (Invitrogen).

2.2 Methods

2.2.1 Preparation of PF127/CA@pMNCs. pMNCs were prepared by a co-precipitation method at 80 °C, with slight modifications.[18] A stoichiometric ratio of 1/1.66 of $FeSO_4{\cdot}7H_2O$ and $FeCl_3{\cdot}6H_2O$ was prepared for each experiment. $FeSO_4{\cdot}7H_2O$, $FeCl_3{\cdot}6H_2O$, and PAA (75–150 mg) were dissolved

individually in deionized water and agitated at room temperature till clear solutions were obtained (10 mL). All the obtained precipitates (after adding 5 mL of NH_4OH) were heated and stirred at 80 °C using a magnetic stirrer at 450 rpm till their hues altered to black. The obtained precipitates were separated by a magnetic decantation process and, subsequently, rinsed several times with deionized water to remove any extra ions and to achieve a neutral pH. Subsequently, CA (360–720 mg) was added to pMNCs, and lastly, each mixture was stirred at 90 °C for further 90 min and then cooled to room temperature. The CA-coated samples were magnetically decanted, rinsed several times with deionized water and then subjected to sonication for 10 min using an ultrasonic bath (Elma E60 H Elmasonic, Schmidbauer GmbH, Germany). The CA-coated pMNCs (CA@pMNCs) were subjected to oven drying at a temperature of 45 °C. Later on, PF127 (50–75 mg) was added to CA@pMNCs (100 mg), and the mixture was then rapidly agitated at 39 °C for 2 h. The samples were rinsed several times with deionized water to eliminate any surplus polymer. They were identified as PF127/CA@pMNCs, separated by a magnetic decantation method, and subsequently dried at 45 °C overnight.

2.2.2 Synthesis of LEN-loaded PF127/CA@pMNCs. First, 1 mg LEN was added to 5 mL of PF127/CA@pMNCs (10 mg) and then probe-sonicated at 130 W for 1 min using a lab probe-sonicator (Heidolph, D-991126, Schwabach, Germany) to enhance the penetration of LEN molecules into the porous assembly of pMNCs to form the PF127/CA/LEN@pMNCs (Fig. S2, ESI†).

2.2.3 Statistical optimization of PF127/CA/LEN@pMNCs. Box-Behnken Design (BBD) created a three-factor, three-level factorial (3^3) approach (Stat-Ease, Minneapolis, MN, USA) using the Design-Expert® software (version 12). Independent variables, namely, PAA (A), CA (B), and PF127 (C) were selected to investigate their effect on the particle size (PS) (*Y*1); polydispersity index (PDI) (*Y*2); zeta potential (ZP) (*Y*3); and %EE (*Y*4) of PF127/CA/LEN@pMNCs at two distinct time points (−1, +1) (Table 1). The final selection of independent variables was based on the given conditions, including PS < 200 nm, PDI (<0.4), maximal ZP, and optimum %EE. Prior reports indicated that formulations possessing these optimal qualities facilitate drug localization at the required site, crossing many physiological barriers, maintaining stability, and enhancing therapeutic effectiveness.[22]

2.3 Characterization of PF127/CA/LEN@pMNCs

2.3.1 PS, PDI and ZP. The PS, PDI and ZP of PF127/CA/LEN@pMNCs were assessed using Zetasizer ZS 90 (Malvern Instruments, Worcestershire, UK) which was equipped with Malvern Software version 6.34.[23] The system employed a laser (Helium-Neon) that operates at 635 nm, at room temperature (25 °C) and at a fixed reflecting angle of 90°.[24] Each sample was measured in triplicate (n = 3).

2.3.2 Evaluation of %EE and drug loading capacity. The %EE of PF127/CA/LEN@pMNCs was assessed using a centrifugation technique. Each sample (1 mL) was centrifuged at 15 000 rpm for 60 min at 4 °C using a Z216 MK centrifuge (HERMLE GmbH, Germany). The resulting supernatant (100 μL) was employed for the estimation of LEN (un-entrapped) by liquid chromatography and mass spectrometry (LC-MS/MS). The LC-MS/MS system comprised a binary pump HPLC (SP LC SP3202, Shiseido, Chuo-ku, Tokyo, Japan) and a Triple Quadrupole Mass Spectrometer (TSQ Quantum™, Thermo Fisher Scientific, Waltham, MA, USA). Additionally, it included an electrospray ionization (ESI) source and a C18 column (3.0 × 100 mm, 2.6 μm, Phenomenex, Torrance, CA, USA). A mobile phase comprising water (containing 0.1% formic acid) and acetonitrile was employed, at a flow rate established at 0.3 mL min^{-1}. The investigation was conducted at 40 °C. Furthermore, ESI was performed in the positive ion mode. Analysis was conducted under optimal conditions, including a spray voltage of 5500 V, ion source gas 1 (60.0 psi), and ion source gas 2 (65.0 psi). Nitrogen gas was provided as a nebulizing agent. The precursor-product ion transitions at m/z 427.1 → 370.0 (LEN) and 432.1 → 370.0 were chosen for the quantification of the internal standard $^2H_5$-LEN due to their sufficient reproducibility and intensity profile.[25] The calibration curves of LEN exhibited a satisfactory linear range of 10–10 000 ng mL^{-1}. Prior to that, the LC-MS/MS methodology for the detection of LEN was developed. The approach demonstrated appropriate linearity with R^2 above 0.999 and a lower limit of quantification (LLOQ) of 0.2 ng mL^{-1} for LEN. Furthermore,

Table 1 Independent variables and responses showed by the Box-Behnken design for pluronic F127-decorated citric acid-capped lenvatinib-loaded porous magnetic nanoclusters (PF127/CA/LEN@pMNCs)

	Levels			
Independent variables	Low (−1)	Medium (0)	High (+1)	Optimized level
A: polyacrylic acid (mg)	75	112.5	150	112.5
B: citric acid (mg)	360	540	720	540
C: pluronic F127 (mg)	50	62.5	75	62.5

Dependent variables	Parameters
*Y*1: particle size (nm)	Decrease
*Y*2: PDI	Decrease
*Y*3: peta potential (mV)	Increase
*Y*4: entrapment efficiency (%)	Increase

mg = milligram; nm = nanometer; mV = millivolt

precision and accuracy were deemed satisfactory within a 20% margin. The findings demonstrated that within and between runs in the precision and accuracy tests were below 15%, which is deemed satisfactory. The following equation was used to obtain the %EE and drug loading capacity of LEN.

$$\text{EE}\,(\%) = \frac{W_t}{W_s} \times 100$$

where W_t is the total quantity of LEN in PF127/CA/LEN@pMNCs and W_s represents the quantity of initial LEN added.

$$\text{Drug loading capacity}\,(\%) = \frac{W_t}{W_u} \times 100$$

where W_u is the total weight of PF127/CA/LEN@pMNCs.

2.3.3 Scanning electron microscopy (SEM). A SEM (S-4800; Hitachi, Tokyo, Japan) was used for the surface morphological assessment of PF127/CA/LEN@pMNCs. The sample was diluted with an aqueous medium, and a small quantity of liquid was located on a glass slide of specifications (1 cm × 1 cm). A vacuum desiccator was used to dehydrate the glass slide, followed by the gold sputtering. The equipment was operated at a voltage of 15 kV and images were acquired at different magnifications.[26,27]

2.3.4 Transmission electron microscopy (TEM). A TEM (Hitachi H-7600; Tokyo, Japan) was used to examine the internal morphology of PF127/CA/LEN@pMNCs. Briefly, PF127/CA/LEN@pMNCs were deposited onto a framework with a copper coating and then marked with a phosphotungstic acid aqueous solution (2%).[28] The samples were dried overnight using an oven, followed by their examination using a TEM at a voltage of 100 kV.[29,30]

2.3.5 Fourier transform infrared spectroscopy. An FTIR spectrometer (Bruker FTIR Spectrometer Alpha II, Massachusetts, USA) was employed to examine the chemical interactions of the PF127/CA/LEN@pMNCs and their components. In this work, potassium bromide pellets were used and the functional group of the test samples were analyzed in the wavenumber ranging from 4000 to 500 cm^{-1}.[31,32]

2.3.6 Thermal behavior. A DSC (TA Instruments, Inc., New Castle, DE, USA) was used to obtain the thermograms of LEN and PF127/CA/LEN@pMNCs. Each sample (5 mg) was precisely measured and taken in an aluminum pan, covered with a lid, and located at the respective positions in the DSC. Increased heating was observed on a heating scale of 30–350 °C at a rate of 10 °C min^{-1}.[33,34]

2.3.7 Crystallinity. The purity and crystallinity of the fabricated formulations were evaluated using a powder X-ray diffractometer (D/MAX-2500 PC, Rigaku Corporation, Tokyo, Japan). Examination was done using Theta-Theta S/N 65 022 with Cu-Kα radiation (λ = 1.54, 40 kV, 30 mA) in the 2θ range from 20 to 90°.[35,36]

2.3.8 Magnetic properties. The magnetic properties of the PF127/CA/LEN@pMNCs were analyzed at room temperature, using a VSM (Cryogenic Ltd, London, UK). For analysis, powdered samples were placed in a container and the outside magnetic field strength was applied in the range of −5 to +5 T.[37]

2.3.9 Surface area and porosity analysis. The PF127/CA/LEN@pMNCs were subjected to BET analysis to compute the surface area and pore size using nitrogen adsorption–desorption isotherms at 77 K. The measurements were conducted using a Micromeritics analyzer (Gemini VII; 2390 Surface Area and Porosity; Micromeritics; Norcross, GA, USA). The samples were degassed before analysis at a temperature of 100 °C, under a nitrogen flow, for 1 h to remove moisture and gases.[16,38]

2.3.10 Thermogravimetric analysis (TGA). TGA was conducted using a thermogravimetric analyzer (Diamond Series, PerkinElmer, USA). The analysis was performed at a temperature in the range of 50 to 820 °C, such that the temperature was increased at a rate of 10 °C min^{-1}, under the influence of nitrogen purging.[20]

2.3.11 Inductively coupled plasma-optical emission spectroscopy (ICP-OES). An ICP-OES (Agilent Technologies 5110-vdv USA) was used to calculate the iron content of the PF127/CA/LEN@pMNCs and compared with pMNCs and CA@pMNCs. In this study, 5 mg of each formulation was used.[39]

2.4 *In vitro* drug release

Dialysis membrane technique was employed to conduct an *in vitro* drug release study of LEN from PF127/CA/LEN@pMNCs and compared with LEN dispersion (LEN-Ds).[40] The concentration of LEN was uniform (2.92 mg mL^{-1}) across all formulations. Analysis was performed using a water bath shaker (Memmert SV, 1422) under continuous agitation at 80 rpm and at a temperature of 37.5 ± 1.0 °C.[41] To examine the pH-sensitive drug release behavior of PF127/CA/LEN@pMNCs, they were added to phosphate-buffered saline (PBS) of pH 7.4 (to mimic arterial blood pH) or pH 5 (to mimic the acidic conditions of the TME pH).[42] To facilitate temperature familiarization, 300 mL of both PBS of pH 7.4 and pH 5 (0.5% Tween 80) were added to two separate 100 mL beakers and then immersed in water.[43] PF127/CA/LEN@pMNCs and LEN-Ds were introduced onto dialysis membranes (Molecular weight = 3500 daltons, Spectrum Laboratories, Inc., Rancho Dominguez, CA USA) that had been soaked beforehand. Each membrane was then placed in beakers filled with a PBS medium of pH 7.4 and pH 5. At intervals of 0.25, 0.5, 1, 2, 4, 6, 12, 24, 36, and 48 h, a total volume of 3 mL sample was collected from every beaker and then replaced with a fresh buffer. The samples were then filtered and analyzed for LEN quantification as discussed above.[25] The cumulative release in percentage *versus* time was evaluated.

2.4.1 Kinetic release models. The DD Solver software was used to examine the outcomes of the *in vitro* release experiment.[44]

Numerous computational models such as zero-order, first-order, Hixson-Crowell, Korsmeyer–Peppas, and Higuchi were applied to determine the drug release kinetics of LEN from the PF127/CA/LEN@pMNCs.[45,46]

2.5 Cytotoxicity assay

The cytotoxicity assay of the PF127/CA/LEN@pMNCs was performed on H22 and Hep3B cells, by an MTT test. The cell viability was observed at different concentrations.[47] Cells were inoculated at a density of 1 × 10^4 cells per well (100 μL) in

96-well plates and incubated for 24 h in a CO_2 chamber (5%) at 37 °C. Following 24 h of incubation, 20 μL of MTT solution (5 mg mL^{-1}) was introduced to each well. The cells were cultured again for 4 h, under the mentioned conditions. Media was eliminated, and 200 μL of DMSO was used to solubilize the formazan crystals. The absorbance of the dissolved formazan was quantified at 570 nm using a microplate reader (FLUOstar Omega, BMG LABTECH, Ortenberg, Germany). The analysis was performed in triplicate (n = 3). The percentage of cell viability was assessed,[4,48] and the IC_{50} values were determined using the GraphPad Prism software (version 10).

$$\%\ \text{Cell viability} = \frac{\text{Absorbance of cells treated}}{\text{Absorbance of cells untreated}} \times 100$$

2.6 LDH assay

The MTT assay was cross-validated by an LDH release assay, which was performed using an LDH cytotoxicity assay kit (Beyotime Biotechnology, Shanghai, China). LDH released into the medium of cells treated with test formulations including PF127/CA@pMNCs, LEN-Ds, and PF127/CA/LEN@pMNCs at 5 μg mL^{-1} concentration on H22 and Hep3B cell lines, was investigated. The absorbance was measured at 450 nm. The release of LDH into the cell culture medium was calculated as the percentage of total LDH release after cell lysis, as reported earlier.[49,50]

2.7 Hemolytic assay

Hemolysis study was performed in 1 mL red blood cells (RBC) obtained from Sprague-Dawley rats. Animal studies were performed as per the NIH and ARRIVE guidelines (Version 2) and were approved by the Bioethical Committee of Quaid-i-Azam University Islamabad, Pakistan *via* protocol# BEC-FBS-QAU2021-325. Blood was placed in the K2-EDTA tubes followed by centrifugation at 1500 rpm for 10 min. Later on, the debris and proteins from the collected supernatant were eliminated by rinsing it thrice with PBS (pH of 7.4). Afterwards, a sample containing a dispersion of 50 μL of RBC in 950 μL of PBS (pH 7.4) was prepared. Simultaneously, different concentrations (5, 10, 50, 100, 200, and 400 μg mL^{-1}) of PF127/CA/LEN@pMNCs were prepared and then added to 50/950 μL (v/v) of blood in PBS. All collected dispersions were then subjected to centrifugation for approximately 20 min at 12 000 rpm (37 °C). In this work, 1% Triton X-100 was used as the positive control, while PBS was used as the negative control. The supernatant from all dispersions was shifted to 96-well plates for analysis at a respective wavelength of 540 nm.[51] The % hemolysis was measured using the following standard formulae:[41]

$$\%\ \text{Hemolysis} = \frac{A_{\text{sample}} - A_{\text{negative control}}}{A_{\text{positive control}} - A_{\text{negative control}}} \times 100$$

2.8 Magnetic hyperthermia (MH) analysis

The MH analysis was performed on the PF127/CA/LEN@pMNCs at different concentrations ranging from 5 to 100 mg mL^{-1} at an alternating current magnetic field (AMF) ranging from 165 Oe and a fixed frequency of 330 kHz generated using a COMDEL CLF-5000 USA RF generator (Gloucester, MA, USA).[52] Circulating water was distributed to preserve the temperature of the field coils, ensuring it remained below 20 °C. The heating graphs were generated by plotting the relationship between temperature and time. The SAR that determines the heating efficiency of PF127/CA/LEN@pMNCs was calculated using the following prescribed formula:

$$\text{SAR} = \frac{cM}{m} \times \frac{\mathrm{d}T}{\mathrm{d}t}$$

where c is the specific heat of the sample, M is the mass of the total sample (grams), and m is the mass of MNPs (grams).[35] In addition, $\mathrm{d}T/\mathrm{d}t$ represents the early linear slope of the treated sample temperature profile obtained by linear fitting of the investigational data during a period.

2.9 Cytotoxicity *via* hyperthermia treatment (HT)

This study was performed to investigate the effect of magnetic hyperthermia on the antitumor performance of PF127/CA/LEN@pMNCs (5 μg mL^{-1}) in H22 and Hep3B cells. The analysis was conducted in an alternating magnetic field (AMF) established using EASYHEAT 8310 (Ambrell, NY, USA) with previously defined safety parameters for 30 and 60 min.[53] The magnetic fluid (PF127/CA/LEN@pMNCs) was diluted with Dulbecco's modified Eagle's medium (DMEM). H22 and Hep3B cells were cultivated in 35 mm culture dishes, subjected to 5 μg mL^{-1} concentration of magnetic fluid for 24 h, and subsequently positioned within 2 × 2 turns of Helmholtz coils with an inner diameter of 60 mm and a frequency of 330 kHz (Ambrell, NY, USA) in a wooden Class II/A2 biosafety cabinet under controlled temperature and pressure. The procedure entailed inoculating 0.25×10^6 cells across six culture dishes designated as follows: (1) control without PF127/CA/LEN@pMNCs and HT; (2) cells without PF127/CA/LEN@pMNCs subjected to 30 min of HT; (3) cells without PF127/CA/LEN@pMNCs subjected to 60 min of HT; (4) cells with PF127/CA/LEN@pMNCs subjected to 30 min of HT; (5) cells with PF127/CA/LEN@pMNCs subjected to 60 min of HT; and (6) cells with LEN-Ds subjected to 60 min of HT. The inoculated cells were incubated in a CO_2 chamber (5%) at 37 °C for 24 h. A magnetic field of 15.3 kA m^{-1} was established and maintained to attain a temperature range of 44 ± 1 °C throughout the experiment. Thereafter, the cells were evaluated for viability, as discussed earlier in Section 2.5.

2.10 Statistical analysis

The experimental results were expressed as average ± SD, considered significantly different at $^*p < 0.05$. The statistical optimization of PF127/CA/LEN@pMNCs was conducted using Design-Expert® through the statistical technique, *i.e.*, analysis of variance (ANOVA). The techniques used for the assessment of statistics on the data include the *post-hoc* Tukey test. The GraphPad Prism software (Version 10, San Diego, USA) was used to measure the IC_{50} values. The methodology adopted was to collect the percent viability data at each concentration, normalize data, apply non-linear regression, select dose-response inhibition (log inhibitor) *vs.* normalized response-variable slope, and

then measure the best-fit value (IC_{50}). In addition, the Origin® 2018 graphing and analysis software and Sigma plot (version 15) were used to create many figures based on the information provided in this research work.

3 Results

3.1 Statistical analysis of 3^3 BBD

The prepared formulations were assessed for various physicochemical responses (Table 2). The optimal model recommended for the variables *Y*1, *Y*2, and *Y*4 was quadratic, while *Y*3 was modeled as 2F1. The *p*-values for *Y*4 were reflected as statistically significant ($p < 0.05$). However, for *Y*1, *Y*2, and *Y*3, the *p*-values were insignificant ($p > 0.05$), yet the results were promising. The *F*-values for *Y*1, *Y*2, *Y*3, and *Y*4 were 0.43, 0.63, 1.60, and 5.87, respectively. These values indicated that the model was significant, specifically with *Y*4. All of the proposed models exhibited a lack of fit insignificant as compared to the pure error.[54]

3.1.1 Evaluation of PS. The PS of the PF127/CA/LEN@pMNCs ranged from 79.09 ± 3.16 nm to 999.95 ± 193.82 nm (Table 2). The ANOVA specified that the independent variables (PAA and CA) had a noteworthy effect on the average PS ($p > 0.05$). The impact of the selected independent factors (*A*, *B*, and *C*) on the PS of PF127/CA/LEN@pMNCs was effectively illustrated by the utilization of 3D surface model graphs (Fig. 1A). Additionally, the polynomial equation provided below for regression was another contributing component in comprehending the effect of independent variables on the PS:

$$Z1 = 532 + 49.4063A + 56.38B + 89.4763C - 73.6AB + 115.737AC + 62.265BC - 34.8988A^2 - 186.276B^2 - 150.339C^2$$

Moreover, the R^2 value of 0.3584 indicates a lack of correlation, and the expected adequate precision of 1.89 suggests an insufficient signal. Hence, it is not desirable to apply this model for navigating the design space.

3.1.2 Evaluation of PDI. The PDI of the PF127/CA/LEN@pMNCs ranged from 0.297 ± 0.017 to 0.790 ± 0.217 (Table 2). The ANOVA revealed that PAA and CA had a promising impact on the PDI ($p > 0.05$). The impact on the PDI of PF127/CA/LEN@pMNCs was effectively illustrated using 3D surface model graphs (Fig. 1B), as well as by the polynomial equation for regression provided as follows:

$$Z2 = 0.59 + 0.01625A + 0.0375B + 0.07875C - 0.055AB - 0.0025AC + 0.07BC - 0.00375A^2 - 0.11625B^2 - 0.05875C^2$$

In addition, the R^2 value deviated significantly from 1, with a value of 0.4482, while the likely adequate precision of 2.38. A ratio of adequate precision (2.38) signified an inadequate signal, thereby suggesting that the model was not appropriate for navigating the design space.

3.1.3 Measurement of ZP. The ZP of PF127/CA/LEN@pMNCs ranged from −18.55 ± 0.07 mV to −34.05 ± 2.61 mV (Table 2). The ANOVA revealed that both PAA and CA have demonstrated meaningful effects on the ZP ($p > 0.05$). The outcomes of the independent variables on the ZP of PF127/CA/LEN@pMNCs were elucidated by the utilization of 3D surface model graphs (Fig. 1C). The subsequent polynomial equation for ZP demonstrated its correlation with the variables *A*, *B*, and *C*.

$$Z3 = -27.0912 - 0.7875A - 2.61875B + 1.61875C - 4.2875AB - 2.0875AC + 0.775BC$$

In addition, the R^2 value of 0.4899 specified that the current model was not a strong analyst of the response variable. The adequate precision ratio of 5.055 proposed that the signal was sufficient. This model was applicable for navigating the design space.

3.1.4 Estimation of %EE. The %EE of LEN loaded in the pMNCs ranged from 75.44% ± 0.67% to 98.13% ± 0.51% (Table 2). The ANOVA revealed that only PAA had a statistically significant impact on the %EE ($p < 0.05$). The impacts seen on the independent variables were visible from the 3D surface graphs (Fig. 1D), as well as from the polynomial equation described as follows:

Table 2 Statistical optimization of the pluronic F127-decorated citric acid-capped lenvatinib-loaded porous magnetic nanoclusters (PF127/CA/LEN@pMNCs) using the Box-Behnken model through Design-Expert®

	Formulation constituents			Characterization			
Run	PAA (mg)	CA (mg)	PF127 (mg)	Particle size (nm)	PDI	Zeta potential (mV)	%EE (LEN)
S1	75	540	75	183.25 ± 1.76	0.511 ± 0.048	−18.55 ± 0.07	94.78 ± 0.62
S2	150	360	62.5	161.90 ± 30.54	0.382 ± 0.021	−19.35 ± 0.21	90.96 ± 0.18
S3	112.5	360	50	239.50 ± 2.96	0.413 ± 0.016	−23.25 ± 0.63	91.61 ± 0.98
S4	75	720	62.5	606.95 ± 698.69	0.670 ± 0.466	−24.35 ± 2.75	78.23 ± 0.16
S5	112.5	540	62.5	160.90 ± 5.51	0.371 ± 0.036	−22.80 ± 0.70	98.13 ± 0.51
S6	112.5	720	50	79.09 ± 3.16	0.297 ± 0.017	−34.05 ± 2.61	83.35 ± 0.35
S7	112.5	720	75	275.80 ± 45.53	0.563 ± 0.091	−32.30 ± 2.12	79.40 ± 0.53
S8	75	540	50	129.00 ± 20.22	0.325 ± 0.001	−29.00 ± 0.56	92.07 ± 0.18
S9	112.5	360	75	187.15 ± 1.62	0.405 ± 0.046	−24.60 ± 0.42	75.44 ± 0.67
S10	150	540	75	796.00 ± 49.78	0.732 ± 0.070	−29.65 ± 2.33	94.30 ± 0.02
S11	150	720	62.5	276.10 ± 6.92	0.408 ± 0.045	−29.15 ± 4.17	96.77 ± 0.48
S12	150	540	50	278.80 ± 57.84	0.557 ± 0.024	−31.75 ± 0.21	96.36 ± 0.13
S13	75	360	62.5	198.35 ± 14.21	0.430 ± 0.096	−31.70 ± 3.39	95.56 ± 0.09

PAA = polyacrylic acid; CA = citric acid; PF127 = pluronic F127; PDI = polydispersity index; %EE = percent entrapment efficiency; LEN = lenvatinib; mg = milligram; nm = nanometer; mV = millivolt. Values show mean ± standard deviation.

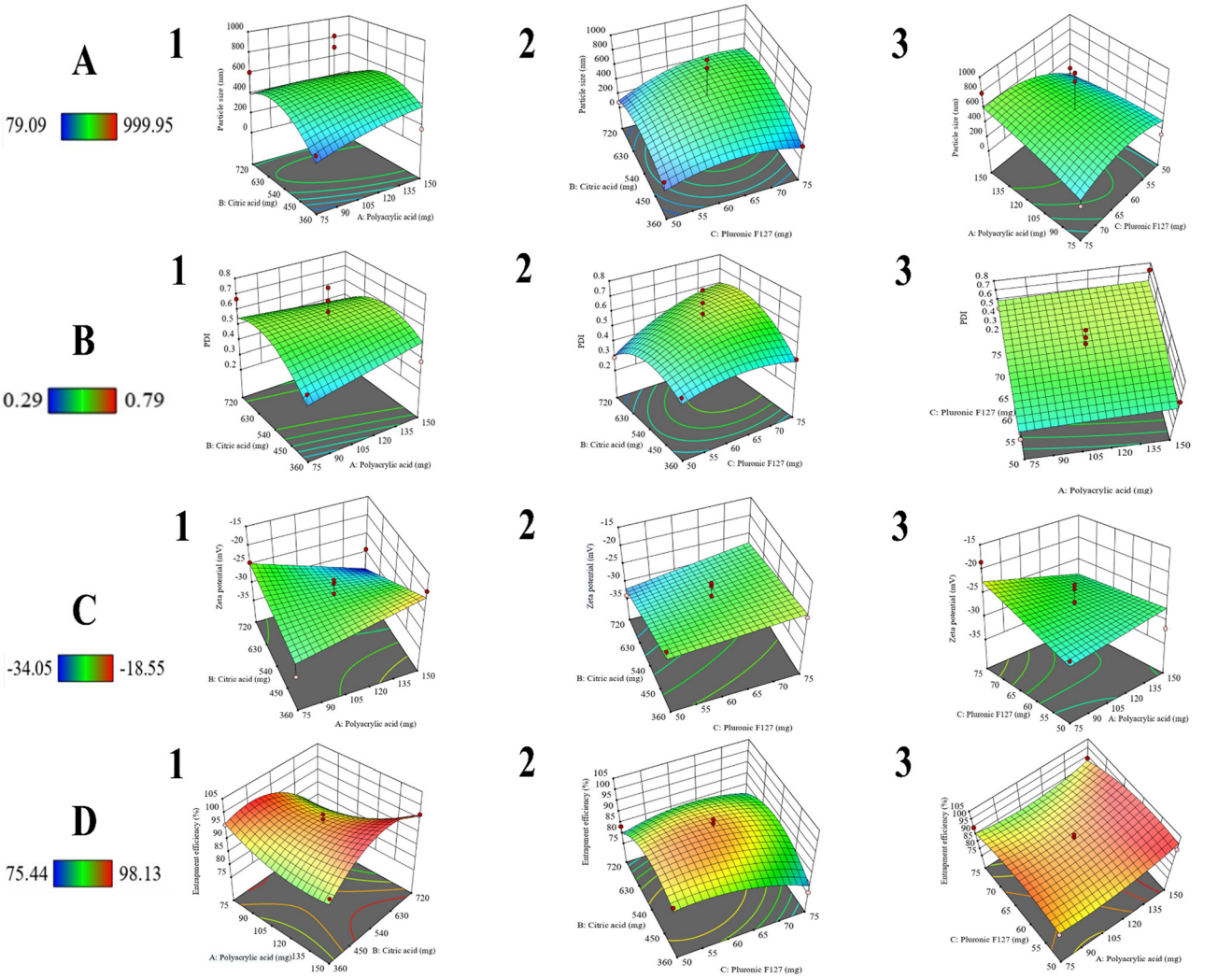

Fig. 1 Three-dimensional surface graphs using response surface methodology. (A) Effect on particle size: (1) impact of polyacrylic acid and citric acid, (2) impact of pluronic F127 and citric acid, and (3) impact of polyacrylic acid and pluronic F127. (B) Effect on PDI: (1) impact of polyacrylic acid and citric acid, (2) impact of pluronic F127 and citric acid, and (3) impact of polyacrylic acid and pluronic F127. (C) Effect on zeta potential: (1) impact of polyacrylic acid and citric acid, (2) impact of pluronic F127 and citric acid, and (3) impact of polyacrylic acid and pluronic F127. (D) Effect on entrapment efficiency: (1) impact of polyacrylic acid and citric acid, (2) impact of pluronic F127 and citric acid, and (3) impact of polyacrylic acid and pluronic F127.

$$Z4 = 94.964 + 2.21875A - 1.9775B - 2.43375C + 5.785AB - 1.1925AC + 3.055BC + 3.67175A^2 - 8.25575B^2 - 4.25825C^2$$

Moreover, the R^2 value of 0.8831 demonstrated a high level of acceptance for the suggested quadratic model. The adequate precision ratio of 7.559 proposed that the signal was sufficient. This model was applicable for navigating the design space.

3.1.5 Statistically optimized PF127/CA/LEN@pMNCs. The optimized PF127/CA/LEN@pMNCs (Run-S5) achieved a desirable PS (160.90 ± 5.51 nm) (Fig. 2A) with a narrow size distribution (PDI of 0.371 ± 0.036) and a reasonable surface charge (ZP of −22.80 ± 0.70 mV) (Fig. 2B). Moreover, it showed a high %EE (98.13% ± 0.51%) and drug loading capacity (8.90%).

3.2 Morphological analysis

The SEM micrographs of PF127/CA/LEN@pMNCs displayed nanoclusters with quasi-spherical forms and rough surfaces. They exhibited reduced aggregation and had a size ranging from 50 to 100 nm (Fig. 2C). The TEM images verified that the MNPs were clustered, forming distinct boundaries (Fig. 2D), and had an approximate size of 100 nm.

3.3 FTIR analysis

In the spectra of PAA, characteristic peaks at 1710 cm^{-1} and 1400–1450 cm^{-1} were attributed to the carbonyl group and stretching of the C–O bond; the characteristic peaks at 1150–1280 cm^{-1} were assigned to the presence of aliphatic acid.[55] Moreover, the wideband spectrum at 3411 cm^{-1} was ascribed to the O–H group of absorbed water molecules. Regarding the spectra of pMNCs, the characteristic peaks at 1567 and 1406 cm^{-1} were attributed to the carboxylate COO group, and a wide peak at 3408 cm^{-1} indicated the chemisorption of PAA onto iron oxides. Moreover, the band appearing at 609 cm^{-1} resembles the absorption of Fe–O bonds.[56] In the spectra of CA,

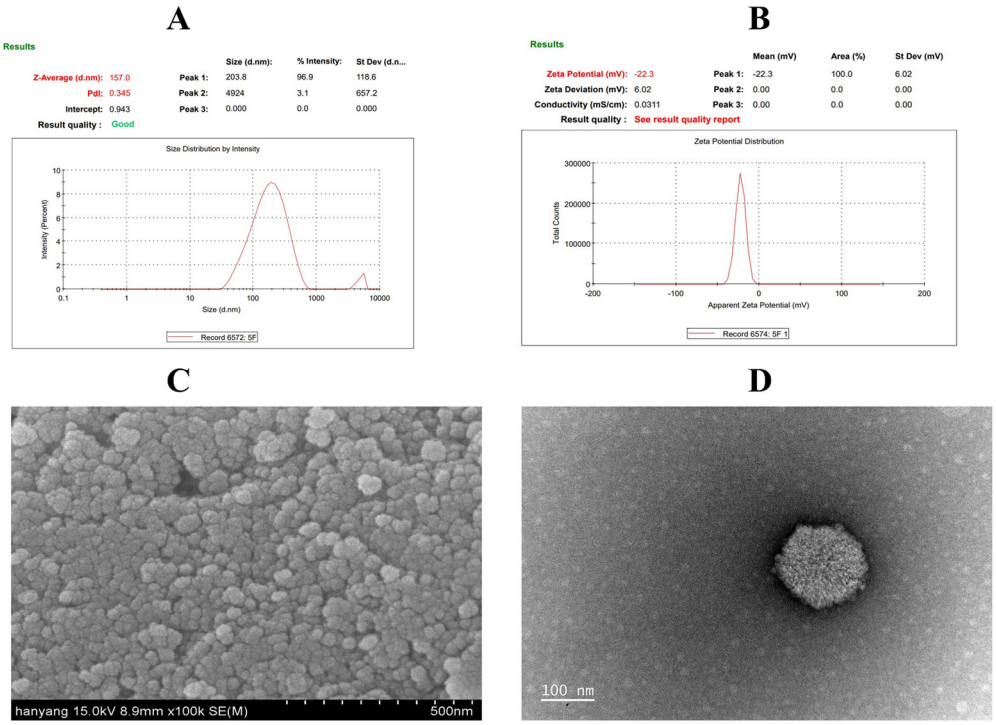

Fig. 2 Characterization of pluronic F127-decorated citric acid-capped lenvatinib-loaded porous magnetic nanoclusters (PF127/CA/LEN@pMNCs): (A) analysis of particle size; (B) measurement of zeta potential; assessment of morphology *via* (C) scanning electron microscopy and (D) transmission electron microscopy.

the characteristic peaks at 3000 cm^{-1} were attributed to the OH group[57] and the characteristic peaks at 1720 cm^{-1} were credited to the C=O bond in the –COOH group.[18] Moreover, the carboxylate group showed asymmetrical and symmetrical stretching vibrations at 1547 cm^{-1} and 1386 cm^{-1}.[57] In the spectra of CA@pMNCs, the characteristic peaks at 2900 cm^{-1} were attributed to the C–H bond; characteristic peaks of 1720 cm^{-1} in CA have migrated to a lesser wavenumber of 1622 cm^{-1} due to the attachment of CA radicals on the surface of nanoclusters by the chemisorption of carboxylate citrate ions.[18] Besides, characteristic peaks at 1461 cm^{-1} were attributed to CO in the carboxylic group.[18] In the spectra of PF127, the characteristic peaks at 1100 cm^{-1} were attributed to the C–O–C stretching vibration mode of the PPO/PPE chains;[18] the characteristic peaks at 2900–3000 cm^{-1} were attributed to C–H stretching.[58] Regarding, the spectra of PF127/CA@pMNCs showed both CA and PF127 peaks incorporated in it (Fig. 3). In the LEN spectra, the characteristic peaks at 1297 cm^{-1} were attributed to the C–N bonds in the pyridine ring; the characteristic peaks at 3335 cm^{-1} were attributed to the N–H bond in the primary amine. Moreover, the characteristic peaks at 3177 and 2980 cm^{-1} were attributed to the N–H bond in the secondary amine. Additionally, the peak at 1660 cm^{-1} was assigned to the C=O stretching vibration.[59] In the spectra of PF127/CA/LEN@pMNCs, the mentioned peaks were aligned with the effective incorporation of LEN, as a noted peak at 1297 cm^{-1} resembles the C–N stretching vibration, which was the characteristic peak of LEN (Fig. 3).

3.4 DSC analysis

Fig. 4A shows the DSC thermograms of LEN and PF127/CA/LEN@pMNCs. A sharp and distinct endothermic peak of LEN was observed at 241.02 °C, representing its melting point.[59] The peaks of LEN in PF127/CA/LEN@pMNCs were not detectable, suggesting that LEN had been entangled inside the porous structure of pMNCs, possibly in an amorphous or disordered crystalline state.

3.5 XRD analysis

XRD findings are displayed in Fig. 4B. As can be seen, pMNCs exhibited multiple peaks at 2θ angles, including 30.14°, 35.38°,

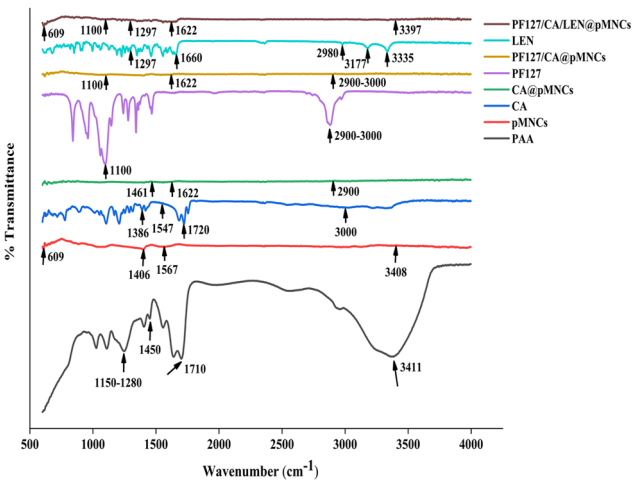

Fig. 3 FTIR spectra of polyacrylic acid (PAA), bare porous magnetic nanoclusters (pMNCs), citric acid (CA), citric acid-capped porous magnetic nanoclusters (CA@pMNCs), pluronic F127 (PF127), pluronic F127-decorated citric acid-capped porous magnetic nanoclusters (PF127/CA@pMNCs), lenvatinib (LEN), pluronic F127-decorated citric acid-capped lenvatinib-loaded porous magnetic nanoclusters (PF127/CA/LEN@pMNCs).

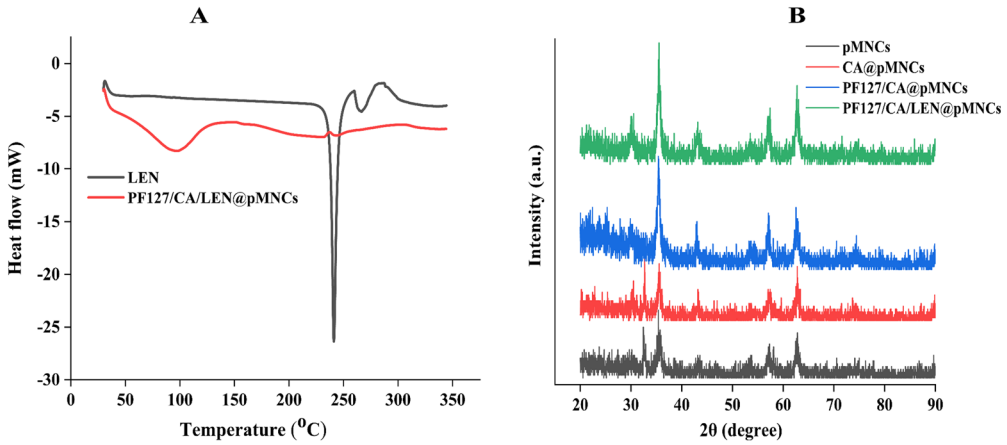

Fig. 4 (A) Diffraction scanning calorimetry (DSC) thermograms of pure lenvatinib (LEN) and pluronic F127-decorated citric acid-capped lenvatinib-loaded porous magnetic nanoclusters (PF 127/CA/LEN@pMNCs). (B) X-ray diffraction patterns of the bare porous magnetic nanoclusters (pMNCs), citric acid-capped porous magnetic nanoclusters (CA@pMNCs), pluronic F127-decorated citric acid-capped porous magnetic nanoclusters (PF127/CA@pMNCs), and pluronic F127-decorated citric acid-capped lenvatinib-loaded porous magnetic nanoclusters (PF127/CA/LEN@pMNCs).

43.14°, 53.56°, 57.29°, and 62.79°. These peaks correspond to the inverse spinal structure of magnetite, as identified by the Joint Committee on Powder Diffraction Standard (JCPDS) reference database (JCPDS no. 19-0629) (Table S1, ESI†).[60] The diffraction peaks in both pMNCs and CA@pMNCs were distinct and well defined, except for a small peak at around 32°, which could be attributed to hematite Fe_2O_3.[61] Additionally, PF127/CA/LEN@pMNCs did not show the characteristic peaks related to LEN, suggesting that LEN was present in an amorphous state within PF127/CA/LEN@pMNCs, which aligns with our DSC findings.

3.6 Magnetization analysis

The Ms values of pMNCs, CA@pMNCs, PF127/CA@pMNCs, and PF127/CA/LEN@pMNCs at 25 °C were 60.606, 51.474, 69.381, and 61.945 emu g^{-1} Fe, respectively (Fig. 5A). The adsorption investigation conducted using a NdFeB permanent magnet provided additional evidence of the significant magnetic responsiveness of PF127/CA/LEN@pMNCs (Fig. 5Aa). This can be attributed to the greater magnetization per particle resulting from the clustering of Fe_3O_4 NPs.

3.7 BET analysis

The PF/127/CA/LEN@pMNCs exhibited a type-IV isotherm (Fig. 5B), indicating the presence of a mesoporous structure and their use as efficient drug delivery systems.[16] The surface area of the PF127/CA/LEN@pMNCs was discovered to be 51.05 m^2 g^{-1}. The PF127/CA/LEN@pMNCs were seen to have a wide area, ranging from 6 to 19 nm (Fig. 5Bb). These sizes

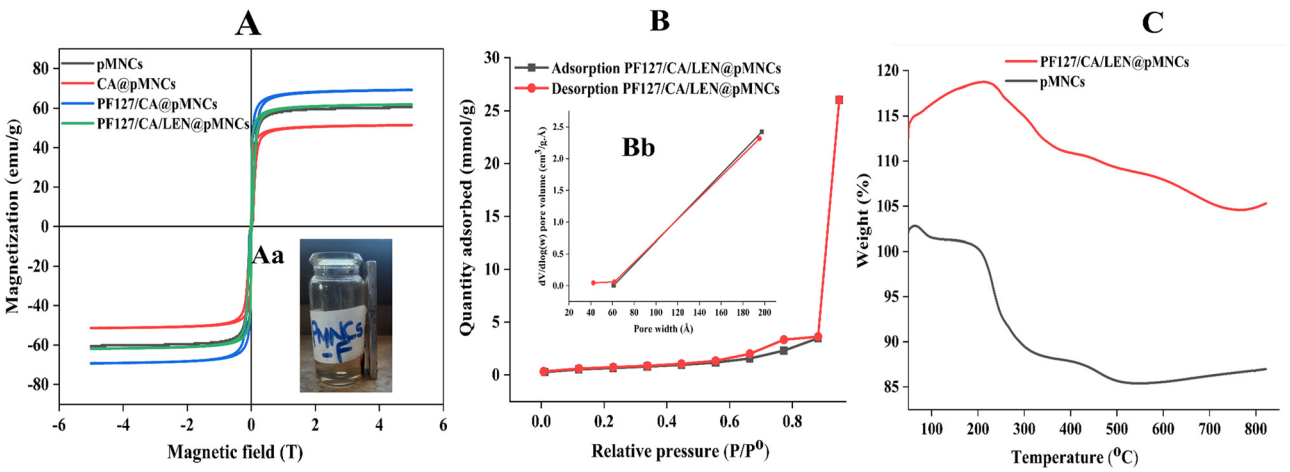

Fig. 5 (A) Magnetization curve of bare porous magnetic nanoclusters (pMNCs), citric acid-capped porous magnetic nanoclusters (CA@pMNCs), pluronic F127-decorated citric acid-capped porous magnetic nanoclusters (PF127/CA@pMNCs) and pluronic F127-decorated citric acid-capped lenvatinib-loaded porous magnetic nanoclusters (PF127/CA/LEN@pMNCs). Fig. 5Aa shows the magnetic responsiveness of PF127/CA/LEN@pMNCs. (B) Type IV adsorption–desorption isotherm and Fig. 5Bb indicates the pore size-distribution results measured from the BJH adsorption and desorption pore volume experimental data for the pluronic F127-decorated citric acid-capped lenvatinib-loaded porous magnetic nanoclusters (PF127/CA/LEN@pMNCs). (C) Thermogravimetric analysis of bare porous magnetic nanoclusters (pMNCs) and pluronic F127-decorated citric acid-capped lenvatinib-loaded porous magnetic nanoclusters (PF127/CA/LEN@pMNCs) performed in an N_2 environment.

correspond to the presence of small size pores within MNPs that make up the nanoclusters and mesopores that represent the interspace area between the Fe_3O_4 nanoclusters.

3.8 TGA

An initial weight loss of 1.20% was detected in the thermogram of pMNCs at temperatures up to 100 °C. This reduction could be accredited to the removal of water molecules that were adsorbed onto the material. Moreover, it showed a 16.21% weight loss due to the breakdown of carboxyl groups in PAA.[16] Further weight gain was observed beyond 550 °C because of the oxidation of MNPs. Regarding PF127/CA/LEN@pMNCs, an initial observation revealed an unforeseen increase in weight, which could potentially be attributed to the oxidation of MNPs that occurred at a temperature in the range of 130 to 210 °C. Moreover, it showed a total of 14.14% weight loss. The TGA measurements have verified the coating of CA and PF127 on the surface of the pMNCs (Fig. 5C). The sudden increase in weight following 750 °C may be attributed to the oxidation of MNPs.

3.9 ICP-OES examination

The ICP-OES examination verified that the superparamagnetic pMNCs were entrapped within the assembled ones. The Fe concentration in pMNCs was 64.36%, whereas in CA@pMNCs, it was significantly higher (83.91%). The PF127/CA@pMNCs had a quantity of 70.05%, and in PF127/CA/LEN@pMNCs, the iron quantity remained within acceptable limits at 55.78%. The iron content of respective formulations falls within the acceptable range of 55.78–83.91%.[39]

3.10 *In vitro* release profiles

In vitro release profiles of LEN-Ds and PF127/CA/LEN@pMNCs are displayed in Fig. 6. *In vitro* release at pH 7.4 showed that the release rate of LEN reached 94% within 24 h and then remained stable from LEN-Ds, demonstrating a rapid release rate of the unencapsulated drug (Fig. 6A). However, the PF127/CA/LEN@pMNCs significantly retarded the drug release, as around 38% LEN was released within 24 h. Moreover, a total of 47% LEN was observed to be released in 48 h, indicating the ability of the nanocluster to control the drug release. At pH 5, a comparatively fast release of LEN was observed from both formulations (Fig. 6B). As indicated, above 90% drug was released from LEN-Ds in 6 h followed by more than 99% of drug releases in 24 h. Nevertheless, around 72% and 84% of LEN was released from the PF/127/CA/LEN@pMNCs after 24 and 48 h, respectively. The drug-release time of LEN encapsulated by pMNCs was significantly prolonged at both pH levels, indicating the sustained-release effect of PF127/CA/LEN@pMNCs. Additionally, a notable increase in drug release at pH 5 as compared to pH 7.4 (Fig. 6C) is desirable for achieving the therapeutic effect of LEN in the TME.

3.10.1 Measurement of kinetic release models. The LEN release pattern of PF127/CA/LEN@pMNCs at both pH values followed the Korsmeyer–Peppas kinetic model, as indicated by the high R^2 value approaching 1 (Table 3). Moreover, the measured value of n indicated that the pattern of release followed the Fickian diffusion at both pH 7.4 and 5 (n value less than 0.5).

3.11 *In vitro* cell line study

3.11.1 H22 cell line study. The H22 cell line results indicated a minimal reduction in cell viability when exposed to PF127/CA@pMNCs. The cell count was decreased from 98.00% ± 1.30% to 92.01% ± 3.16% at 0.5 μg mL^{-1} and 100 μg mL^{-1}, respectively. Nevertheless, the viability in LEN-Ds and PF127/CA/LEN@pMNCs decreased from 65.03% ± 6.23% and 76.13% ± 5.32% at 0.5 μg mL^{-1} to 2.12% ± 0.87% and 3.18% ± 1.08% at 100 μg mL^{-1}, respectively, thereby indicating their potential to eliminate cancer cells when compared with PF127/CA@pMNCs (Fig. 7A). The IC_{50} values of PF127/CA@pMNCs was measured to be 80 427 μg mL^{-1}. In comparison, the IC_{50} values of LEN-Ds and PF127/CA/LEN@pMNCs were calculated to be 7.607 and 4.427 μg mL^{-1}. This assay demonstrated that the IC_{50} value of LEN in PF127/CA/LEN@pMNCs was lowered by roughly 2-fold in H22 cells compared to the free drug.

3.11.2 Hep 3B cell line study. The data from the Hep 3B cell line is presented in Fig. 7B, respectively at 12 h (I), and 24 h (II). It demonstrated that the cell viability of PF127/CA@pMNCs

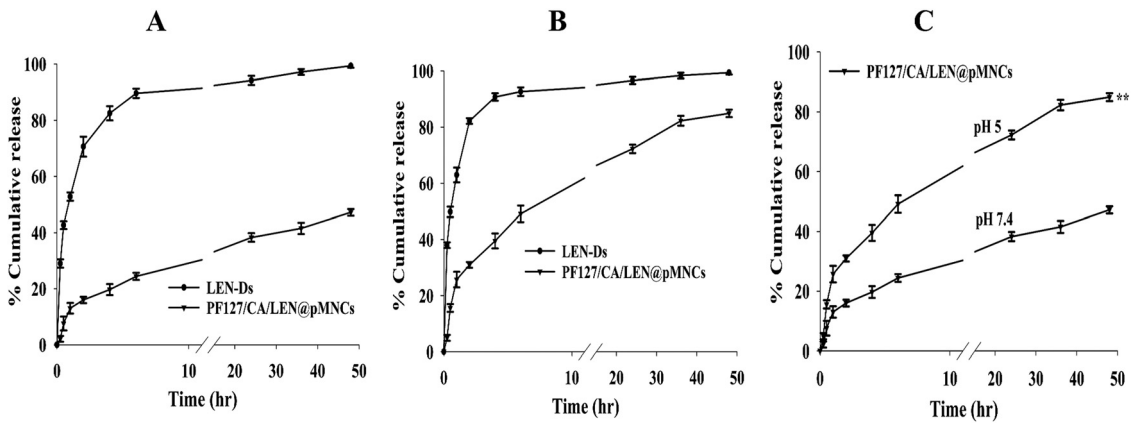

Fig. 6 Lenvatinib release profiles from LEN dispersion (LEN-Ds) and pluronic F127-decorated citric acid-capped lenvatinib-loaded porous magnetic nanoclusters (PF127/CA/LEN@pMNCs) in a buffer with (A) pH value 7.4 and (B) pH value 5. (C) *In vitro* release of PF127/CA/LEN@pMNCs at pH 5 and 7.4. ** significance difference ($p \leq 0.005$), when compared with pH 7.4. Data are represented in triplicate ($n = 3$).

Table 3 Kinetic release models for pluronic F127-decorated citric acid-capped lenvatinib-loaded porous magnetic nanoclusters (PF127/CA/LEN@pMNCs)

R^2 values		
	pH 7.4	pH 5
Zero-order	0.3248	0.1711
First order	0.5130	0.8034
Hixson-Crowell	0.4531	0.7140
Korsmeyer–Peppas	0.9788 (n = 0.360)	0.9673 (n = 0.337)
Higuchi	0.9061	0.8561

was found to be high at 12 h (93.17% ± 2.7%) and 24 h (92.17% ± 2.79%). However, LEN-Ds exhibited cell viability of 43.65% ± 3.12% and 26.21% ± 3.72% after 12 and 24 h, respectively. Similarly, the cells treated with PF127/CA/LEN@pMNCs displayed promising cell viability of 38.78% ± 3.51% and 11.61% ± 3.95% after 12 and 24 h, correspondingly, indicating their substantial capacity to eradicate cancer cells. The IC_{50} values of LEN-Ds and PF127/CA/LEN@pMNCs at 12 h were noted to be 3.87 and 3.18 μg mL^{-1}, while at 24 h, they were 1.85 and 0.85 μg mL^{-1}, respectively. In contrast, the IC_{50} value of LEN in PF127/CA/LEN@pMNCs was decreased by approximately 2-fold as compared to the free LEN. The IC_{50} values of PF127/CA@pMNCs at 12 and 24 h were noted as 41.79 and 38.39 μg mL^{-1}, respectively.

3.12 LDH analysis

The LDH assay was performed to further validate the cytotoxicity of PF127/CA/LEN@pMNCs in HCC cell lines (H22, Hep3B). A significantly increased amount of LDH was released by the PF127/CA/LEN@pMNCs when compared to other test groups (LEN-Ds and PF127/CA@pMNCs) in both the cell lines. Fig. 8A shows that around 66.7% ($p < 0.01$) LDH was released when PF127/CA/LEN@pMNCs were exposed to the H22 cells, followed by LEN-Ds (38.6%) and PF127/CA@pMNCs (6.5%). Similarly, upon exposure to Hep3B cell lines (Fig. 8B), a meaningfully enhanced LDH was released by PF127/CA/LEN@pMNCs (53.1%, $p < 0.01$), as compared to LEN-Ds (27.5%) and PF127/CA@pMNCs (5.1%). These results confirmed the cytotoxic potential of PF127/CA/LEN@pMNCs, thereby indicating the efficacy of the developed formulation in HCC cells.

3.13 Hemolytic assay

The PF127/CA/LEN@pMNCs exhibited no hemolytic activity (0.14%), even at an excessive concentration of 400 μg mL^{-1} (Fig. 9A). It has been reported earlier that hemolysis below 5% is considered safe for biomedical materials, owing to their no toxic manifestation.[62,63] Thus, the PF127/CA/LEN@pMNCs were classified as nonhemolytic materials, thereby having no cytotoxic effects on rat erythrocytes.

3.14 MH assessment

The temperature of the suspensions was increased to 29.73, 33.59, 32.79, 42.40, and 24.84 °C, at colloidal concentrations of 100, 50, 25, 10, and 5 mg mL^{-1}, respectively (Fig. 9B). The SAR values for different concentrations of PF127/CA/LEN@pMNCs are presented in Table S2 (ESI†). Among the tested formulations, PF127/CA/LEN@pMNCs-4 quickly reached the therapeutic temperature range of 41–45 °C for MH treatment and was thus considered the optimized concentration.[64]

3.15 Cell viability under MH influence

This study illustrated the anticancer effectiveness of PF127/CA/LEN@pMNCs in H22 and Hep3B cancer cells when subjected to MH and was compared to control, AMF, and LEN-Ds. No significant change in the viability of cells was noted for the H22 cells (Fig. 10A) and Hep3B cells (Fig. 10B) subjected to control conditions (unexposed cells to AMF) and magnetic field

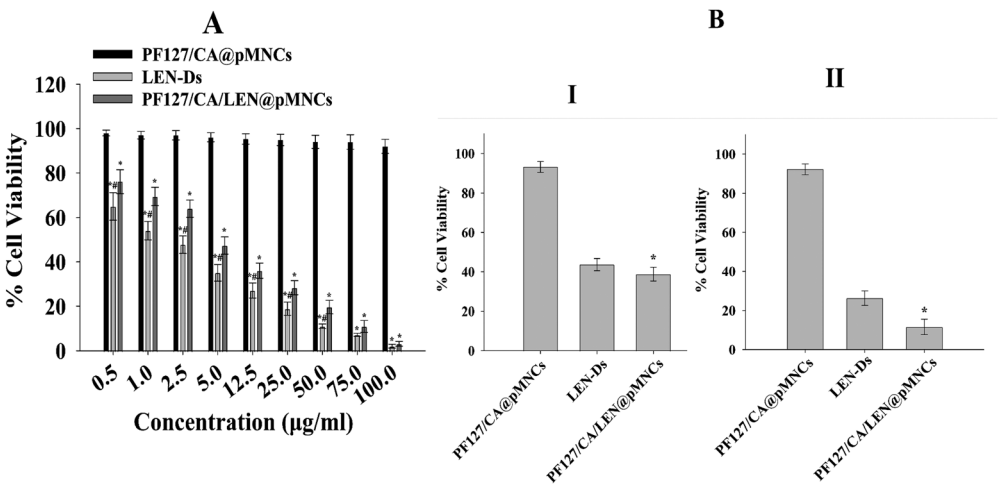

Fig. 7 Cell viability assay at different concentrations of pluronic F127-decorated citric acid-capped porous magnetic nanoclusters (PF127/CA@pMNCs), lenvatinib dispersion (LEN-Ds), and pluronic F127-decorated citric acid-capped lenvatinib-loaded porous magnetic nanoclusters (PF127/CA/LEN@pMNCs) on (A) the H22 cell line and (B) Hep 3B cell line at 12 (I) and 24 h (II). Data are represented in triplicate (n = 3). The statistical significance of the scientific data was examined using a one-way analysis of variance (ANOVA), which was followed by Tukey's *post-hoc* test. * $p \leq 0.05$ when compared with PF127/CA@pMNCs, # $p \leq 0.05$ when compared to PF127/CA@pMNCs and PF127/CA/LEN@pMNCs.

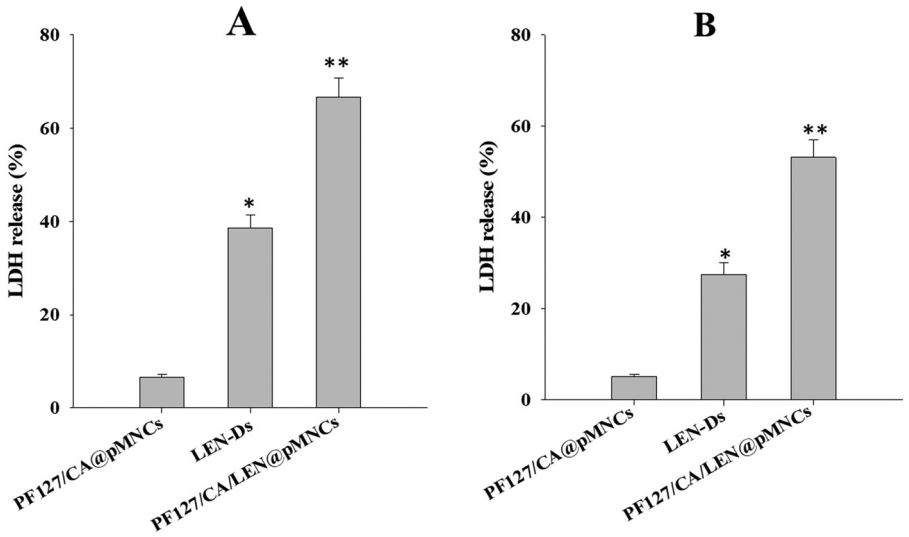

Fig. 8 LDH release assays of PF127/CA/LEN@pMNCs, PF127/CA@pMNCs and LEN-Ds. * $p \leq 0.05$ when compared with PF127/CA@pMNCs, ** $p \leq 0.01$ when compared with PF127/CA@pMNCs and LEN-Ds.

exposure (AMF at 30 and 60 min). However, the H22 and Hep3B cells treated with PF127/CA/LEN@pMNCs in the presence of AMF demonstrated a significant reduction in cell viability. More specifically, 21 and 19% viability of H22 and Hep3B cells was observed after 30 min respectively, and was further reduced to 11 and 2.9% after 60 min, correspondingly (Fig. 10). Conversely, a significantly enhanced cell viability was observed in LEN-Ds-treated cells (both H22 and Hep3B) as compared to PF127/CA/LEN@pMNCs, even if it was significantly reduced compared to the control and AMF groups. These results indicated that PF127/CA/LEN@pMNCs can induce significant cancer cell apoptosis through MFH, attributable to its more heating responses under the applied AMF.

4 Discussion

HCC is characterized by significant vascularity, thereby exhibiting rapid tumor progressing, which may ultimately lead to fatality. Among the available chemotherapeutic agents, LEN is

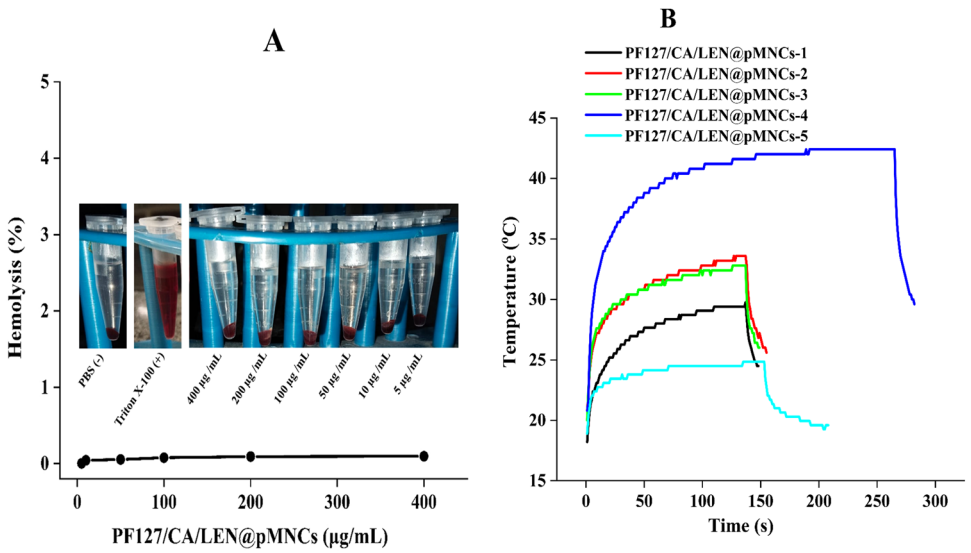

Fig. 9 Percentage hemolysis of erythrocytes (A) when treated with different concentrations of pluronic F127-decorated citric acid-capped lenvatinib-loaded porous magnetic nanoclusters (PF127/CA/LEN@pMNCs). The positive (+) control consists of red blood cells (RBCs) treated with 1% Triton X-100 and the negative (−) control consists of RBCs treated with PBS. (B) Magnetic hyperthermia experiments were conducted on different concentrations of pluronic F127-decorated citric acid-capped lenvatinib-loaded porous magnetic nanoclusters (PF127/CA/LEN@pMNCs). The measurements involved recording the temperature *versus* time of a sample expressed in milligrams per milliliter. The inset displays the original heating curves. Here, PF127/CA/LEN@pMNCs-1, PF127/CA/LEN@pMNCs-2, PF127/CA/LEN@pMNCs-3, PF127/CA/LEN@pMNCs-4, and PF127/CA/LEN@pMNCs-5 represent sample concentrations of 100, 50, 25, 10 and 5 mg mL^{-1}, respectively.

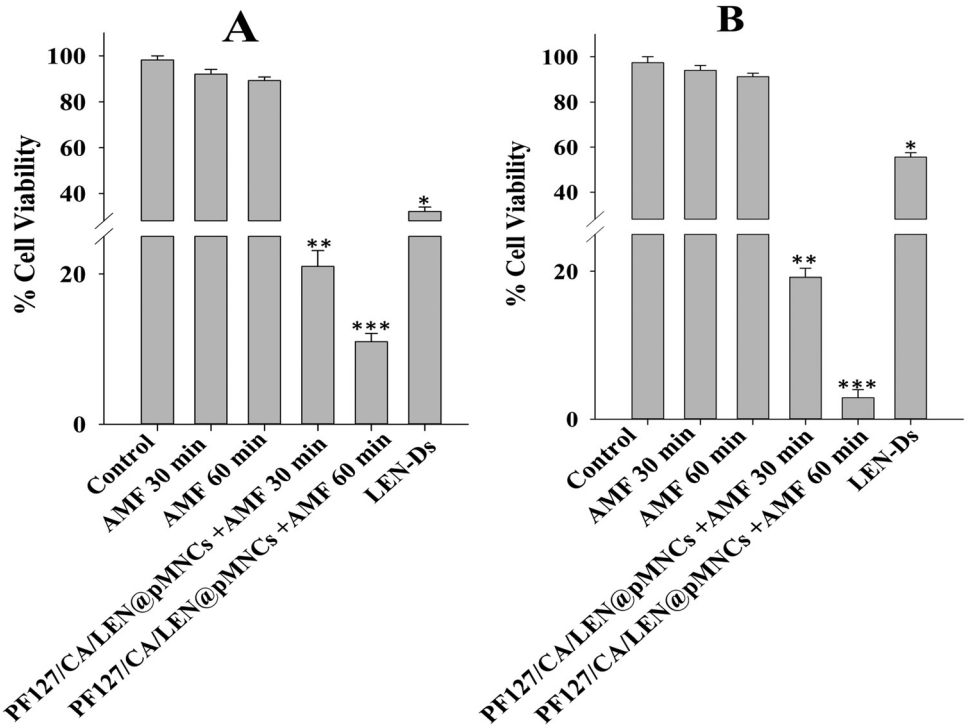

Fig. 10 (A) Cell viability plot illustrating the cytotoxic impact of PF127/CA/LEN@pMNCs on (A) H22 cells and (B) Hep3B cells when exposed to MH conditions at a concentration of 5 μg mL^{-1}. Data are given in triplicate (n = 3). * $p \leq 0.05$ when compared with control and AMF (30 and 60 min). ** $p \leq 0.01$ when compared with control, AMF (30 and 60 min) and LEN-Ds, *** $p \leq 0.001$ when compared with control, AMF (30 and 60 min), LEN-Ds, and PF127/CA/LEN@pMNCs (30 min).

an established therapy for individuals with advanced HCC that cannot be removed by surgery or percutaneous cancer ablation.[16] Nevertheless, the effectiveness of LEN may be constrained by inadequate intracellular drug delivery.[65] There is a need for multifunctional drug delivery carriers that can be used for the treatment of HCC, thereby providing a more precise controlled drug release profile. In this study, pMNCs were produced using an aqueous co-precipitation technique, and subsequently, stabilized electrostatically and sterically by applying double coatings of CA and PF127.

The statistical examination of the investigational data indicates that the close-fitted models exhibited $p < 0.05$ (significant) and lack of fit $p > 0.05$ (non-significant) for the calculated responses. Moreover, increased R^2 values (approaching 1) indicated that the fitted models were proficient in accurately forecasting the responses.[66] Prior research indicated similar results of the optimal model, plus an appropriate precision value (>4), and a difference between adjusted and predicted R^2 values (<0.2).[67] The aforementioned polynomial equations delineate the fitted models based on coded components derived from ANOVA findings. These coded equations are important in determining the comparative influence of the elements by analyzing their coefficients. The coefficients with a p-value less than 0.05 were deemed significant. The positive coefficient in polynomial equations indicated a direct relationship between the independent variable and the response, while the negative coefficient signified an inverse relationship. Excessive PAA was adsorbed on the particle surface, which leads to bridging flocculation.[68] The decrease in PS was due to CA, as it might have stabilized the structure and prevented the aggregation by establishing a dense carboxylate complex with the Fe ions on the external surface.[18] Furthermore, PF127 does not exhibit a favorable effect on PS as a result of the thin polymer coating on the surface, which aligns with our magnetization findings. With the increase in the concentration of PAA, there was a corresponding increase in PDI as a result of greater average PS and a wider distribution. However, the concentration of CA was shown to decrease the PDI by stabilizing the structure through the capping by forming electrostatic interactions between the carboxylate complex and the surface Fe ions, resulting in a better PS distribution.[18] Nevertheless, PF127 does not exhibit any significant effect on PDI. The negative value of ZP was ascribed to the carboxylic groups of PAA and CA. ZP exhibited a rising pattern as a result of the heightened levels of PAA and CA, which guided the configuration of carboxyl groups on the surface. PF127, a non-ionic polymer, is electrically neutral and generally does not affect the ZP of the system. PF127 primarily impacts the steric stability of particles rather than their electrostatic characteristics.[69] The %EE of LEN suggested that LEN was effectively loaded within pMNCs. The %EE was increased by increasing the concentration of PAA due to greater carboxylic groups available for loading LEN by electrostatic interactions with the amino group in LEN molecules.[70]

The optimized formulation (Run-5) exhibited a PS of approximately 160 nm, a PDI of 0.371, and a ZP of −22 mV. NPs fabricated for drug delivery typically range from <200 nm

in size, with controlled release at the desired site of action.[71] The data obtained exhibited a monomodal size distribution. It has been reported earlier that the PDI values below 0.5 confirm the homogeneity and uniform size distribution.[72] Moreover, the presence of ±20 mV potential difference usually enhances the stability of the system, as it causes particles in the dispersion medium to resist each other due to the influence of high negative or positive ZP.[73] As a result of the statistical optimization, the formulation PF127/CA/LEN@pMNCs (Run-S5, Table 2) was identified as the optimal formulation due to its minimized PS (160.90 ± 5.51 nm), suitable PDI (0.371 ± 0.036), adequate ZP (22.80 ± 0.70 mV), and highest %EE (~98%) when compared with the other runs. Moreover, it exhibited high drug loading capacity (8.90%) and better stability owing to its relatively high ZP (Table 2).

The SEM micrographs demonstrated a crumpled surface nanoarchitecture of PF127/CA/LEN@pMNCs characterized by a high level of roughness. In addition, they formed a hierarchical shape characterized by densely packed primary nanocrystals.[74] In addition, TEM analysis confirmed the existence of homogenous solid nanoclusters.[74] It has been reported earlier that smaller particles exhibit an amplified surface area-to-volume ratio, thereby facilitating the penetration of NPs through physiological barriers and accumulation at the tumor site.[22] The spherical shape of PF127/CA/LEN@pMNCs can be attributed to their appropriate composition, nanoscale size, and optimal preparation method. A Zetasizer can precisely measure the hydrodynamic diameter of NPs, leading to an overestimation of their sizes. In this respect, the size was found to be larger than the size determined by SEM (F5, 50–100 nm) and TEM (F5, 100 nm). FTIR findings confirmed the effective synthesis of PF127/CA/LEN@pMNCs and showed that LEN-substituted pMNCs were successfully capped with CA and finally decorated with PF127 properly. Furthermore, no evidence of crystalline LEN was observed following encapsulation and was predominant in an amorphous state, as validated by DSC analysis.[75] The XRD characteristic peaks of pMNCs, CA@pMNCs, PF127/CA@pMNCs, and PF127/CA/LEN@pMNCs were shown to be consistent, indicating that the crystal structure of the PF127/CA/LEN@pMNCs was not affected by the numerous coatings.[76] These findings demonstrated that the coating of the pMNCs with CA and PF127 had no impact on the locations of the diffraction peaks.[18] Moreover, the absence of distinct peaks of LEN suggested that it was present in a non-crystalline form in the PF127/CA/LEN@pMNCs. MNPs must maintain their desirable magnetic characteristics even after coating with polymers to be used as therapeutic agents in MH. Additionally, a sharp slope and the lack of a hysteresis loop in PF127/CA/LEN@pMNCs indicated the superparamagnetic characteristics of the respective formulations at room temperature. This could be credited to the minimal occurrence of remanence and coercivity. The theoretical saturation magnetization for bulk magnetite is approximately 92 emu g^{-1}.[77] However, the magnetite curve demonstrated that this value was decreased to approximately 60 emu g^{-1} for pMNCs. This decrease in Ms may be attributed to the presence of noncollinear spins on the exterior surface of magnetite.[78] The Ms value of pMNCs was dropped from ~60 to ~51 emu g^{-1}, which could be due to the encapsulation of pMNCs by non-magnetic coating with CA. Nevertheless, the superparamagnetic characteristics remained intact during the coating procedure,[79] as demonstrated by Nigam *et al.*, who obtained an Ms value of 57 emu g^{-1} for CA-stabilized MNPs under a magnetic field of 20 kOe.[80] Our results indicated that upon decoration of PF127 to CA@pMNCs, a rise in the Ms value was observed from ~51 to ~69 emu g^{-1}, which could be attributed to the contact potential at the Fe_3O_4–PF127 interface.[81] It exhibited the existence of a thin PF127 coating on the exterior surface of PF127/CA/LEN@pMNCs. Nevertheless, the application of LEN loading might alter the arrangement of atomic spins on the surface, which is induced by the disrupted exchange process, thereby leading to a decreased coordination among the surface spins.[82] Thus, LEN loading decreased the Ms value from ~69 to ~61 emu g^{-1}, although the magnetic properties, specifically superparamagnetism, remained unaffected. The dispersion of PF127/CA/LEN@pMNCs in an aqueous solution was improved by a magnetic field, thereby indicating its potential utilization in magnetically targeted therapy.[83] These synthesized formulations have superparamagnetic properties at room temperature, as required for *in vivo* applications. Our project team is currently focusing on examining the potential of the developed novel drug delivery system to target and treat HCC using magnetic targeting to boost the efficacy of this combined metallic therapeutic paradigm. The above-mentioned characteristic features of PF127/CA/LEN@pMNCs offered a great potential for enhanced MR contrast effects. Additionally, our results depicted the assembly of tiny MNPs into nanoclusters using a PAA binding agent. The clustering process created a very porous area that was filled with PAA having a large number of carboxylic groups. These carboxylic groups have a significant attraction towards LEN, and it possesses an amino group with a pK_a value of 5.05.[79] In contrast, the pK_a value for the carboxylic groups of PAA was 4.8.[16] The occurrence of mesopores and a high concentration shown by carboxylic groups in pMNCs significantly improved the drug loading capacity, reaching approximately 98%. The TGA curve of @pMNCs displayed identifiable regions of weight loss phenomena. The initial weight reduction could be associated with the residual moisture in the sample. The subsequent phase of weight reduction may be attributed to de-carboxylation and anhydride formation within the PAA segments.[84] In contrast, the TGA curve of the PF127/CA/LEN@pMNCs demonstrated reduced weight loss due to better stability of the nanocluster, as the integration of Fe_3O_4 nanoclusters into the CA and PF127 coating increased its thermal stability. This was consistent with the *in vitro* and biocompatibility findings of this study.[85] This study exhibited that the PF127/CA/LEN@pMNCs had appropriate thermal stability, owing to a suitable polymer coating. This phenomenon may help the formulation to display a controlled release profile. The Fe concentration of test formulations was analyzed within the sufficient concentration (55.78–83.91%). It was noted that loading efficiency of Fe_3O_4 in multi-layer formulations was improved with enhancement in temperature.[86]

The findings obtained from *in vitro* release data verified that a more enhanced release pattern was noted at pH 5 and the quantity of LEN released from PF127/CA/LEN@pMNCs at pH 5 was twice as much as that observed at pH 7.4. This demonstrated that a larger quantity of LEN was released under acidic conditions compared to neutral ones. This may be attributed to the LEN pH-dependent solubility and its weakly basic nature (pK_a 5.05).[79] It has been reported earlier that LEN demonstrated higher solubility under acidic pH conditions and decreased solubility under neutral and basic conditions.[59] The pH-responsive characteristics of the metallodrug render it highly suitable as a drug carrier for transporting tiny drug molecules into the acidic TME.[87] These findings indicated that LEN was completely entrapped inside the pMNCs and not adsorbed onto the external surface. Furthermore, PF/127/CA/LEN@pMNCs showed a sustained release profile, which might decrease the need for frequent dose administration and, in turn, may enhance the patient compliance. Compared to LEN-Ds, the drug concentration variation in the blood might be decreased, hence lowering toxicity and adverse effects.[47] Based on this discussion, it can be inferred that the extended drug release of PF127/CA/LEN@pMNCs could be beneficial in increasing the drug's interaction with tumor cells for a longer duration. This may potentially enhance the effectiveness of the anticancer treatment and minimize the cytotoxic potential of the drug on healthy cells.[48,88] In addition, $n < 0.5$ showed Fickian diffusion, and the release pattern of LEN was governed by the combined impact of both swelling and diffusion[89,90] at both pH 7.4 and 5. The cell viability of over 90% of the tumor cells was observed when exposed to PF/127/CA@pMNCs, indicating its biocompatible and non-toxic nature. Moreover, the cell viability percentage was decreased in a dose-dependent way by LEN-Ds and PF/127/CA/LEN@pMNCs. A significant decrease in IC_{50} values suggested an enhanced antitumor potential of LEN, when loaded into pMNCs due to the improved solubility of the drug caused by the nanovesicular effects and sustained release nature, thus improving the antitumor potential of the LEN.[91]

The LDH assay was used to measure the cytotoxicity of the developed formulations by detecting the LDH enzyme, which is released into the surrounding medium when the cells are damaged or lysed. This provides an indication of cell membrane integrity and cell death.[49,50] A significantly improved LDH release by PF127/CA/LEN@pMNCs showed the ability of the developed system to induce apoptosis more than the drug dispersion. This could be attributed to the sustained release of LEN, which may disturb the cell membrane integrity and induce oxidative stress, thereby leading to inflammatory responses. These findings indicated that PF127/CA/LEN@pMNCs were a safer alternative to LEN-Ds. The PF127/CA/LEN@pMNCs exhibited no hemolysis, thereby demonstrating their high level of biosafety.[41]

Recently, MH therapy is applauded in the research domain of tumor treatment. Unlike normal cells, the cancer cells have heightened sensitivity to thermal exposure. At elevated temperatures, they experience direct tissue necrosis, apoptosis, and protein denaturation. Nonetheless, normal cells continued to function normally. Therefore, MH treatment is considered a very effective and beneficial approach in the treatment of HCC. The MH characteristics of the developed clusters were found to have enhanced SAR values, owing to the clustering phenomenon and reduced size of the primary nanoparticles.[19] Moreover, only superparamagnetic particles can sustain the continuous heat transfer necessary for MH. Our results indicated that the temperature required to maintain hyperthermia at a concentration of 5 mg mL^{-1} was comparatively brief. In contrast, it also exhibited a sufficient therapeutic window in a short period, even at a low concentration of 10 mg mL^{-1}. It attained the therapeutic temperature in 191 s and lasted for over 260 s, ultimately reaching 42.4 °C within 3.2 min. Excessive heat (exceeding 60 °C) can rapidly induce irreversible protein damage, resulting in harm to the adjacent tissues. The sustained temperature of 42.4 °C obtained in this may have a therapeutic effect with reduced adverse effects. The examination of MH revealed that the temperature of PF127/CA/LEN@pMNCs-4 increased up to 42.4 °C within 3.2 min before reaching a constant value,[92] which is suitable for localized hyperthermia treatment of cancer.[93] The most effective particles for hyperthermia are precisely those that are polymer-coated, as the relaxation of individual particles within the polymer envelope is likely to enhance the relaxation effect of the coated nanostructures. Moreover, the thermoresponsive nature of PF127 appears to facilitate this process: the contraction of the polymer may improve the rigidity of the matrix, thereby increasing the friction of the MNPs and generating additional heat.[94] The primary cause of heat generation could predominantly be associated with Brownian relaxation modes and Néel relaxation modes.[95] Furthermore, this study accomplished the successful synthesis of PF127/CA/LEN@pMNCs (160 ± 5.51 nm) prepared by an ultrasonic-assisted coprecipitation method, which is an additional benefit. The improved magnetic performance of PF127/CA/LEN@pMNCs-4 was evident in its heating performance, which leads to higher heating rates compared to the other samples. All the above-mentioned findings indicated that PF127/CA/LEN@pMNCs-4 (SAR 10.79 W g^{-1}) has the potential to be a suitable candidate for MH application.[96] As expected, the magnetization cycles mentioned earlier resulted in a notable decrease in SAR due to the application of numerous coatings on the pMNCs, as confirmed by FTIR and also reported by many other researchers.[97] Additionally, some scientists have discovered a low SAR value that was adequate to induce MH,[98,99] with a primary objective to decrease the dosage of drugs in all medical therapies. Efficiently achieving the desired temperature in MH required minimized doses of the MNPs with the maximized SAR.[21] Furthermore, the SAR values escalate with the increase in applied frequency. The values can be enhanced by augmenting the concentration of MNPs with suitable size, magnetic field frequency, and intensity.[100] An adequate estimate is that a sufficient concentration of 5–10 mg of magnetic substance per cm^3 of cancer tissue is suitable for MH application in human patients.[101] However, PF127/CA/LEN@pMNCs-3 exhibited increased SAR, although it failed to reach the desired therapeutic range.

The cell viability analysis of H22 and Hep3B cells under the influence of MH demonstrated a further improved antitumor

potential of PF127/CA/LEN@pMNCs with a notable cytotoxic effect that could be attributed to the MH activity of the prepared formulation. The anti-tumor efficacy of PF127/CA/LEN@pMNCs *via* AMF has augmented 3-fold and 8-fold in H22 and Hep3B cells, respectively, when compared with the LEN-Ds at a constant dose of 5 μg mL^{-1}. The combination of hyperthermia appears to amplify the cytotoxic effects of anti-tumor agents by promoting apoptosis and boosting the efficacy of chemotherapy through increased uptake of cytostatic into tumor cells. Moreover, it may inhibit the repair of tumor cells caused by the anti-tumor drugs.[102] These results were in agreement with Kameda *et al.*'s reports, which indicated that apoptosis was markedly increased when hyperthermia was used in combination with anti-tumor drugs.[103] The experimental results suggest that the dosage of anti-tumor drugs may be reduced when combined with hyperthermia, hence minimizing the associated side effects. Moreover, we chose exposure times of 30 and 60 min owing to their safety limits, as reported earlier by Bhardwaj *et al.* (2020).[53] It is also worth mentioning that several other research groups reported an exposure time up to 24 h in order to investigate the safety of the magnetic nanoparticles in biological systems over prolonged exposure times.[104,105] This discussion concluded that the selected exposure time may not affect the cells to suffer adversely. In addition, it further confirmed the thermal stability of the PF127/CA/LEN@pMNCs, as previously confirmed by TGA. However, more investigations are required to check the effect of high concentrations of MNPs, varied magnetic field and frequency on formulation performance under MH in the *in vivo* testing. Nonetheless, the PF127/CA/LEN@pMNCs were found to exhibit improved antitumor efficacy under MH that could be efficiently used in the treatment of HCC. However, more comprehensive toxicity assessments must be conducted in animal cohorts to enhance safety profiles prior to clinical trials. In this regard, our research group is extending the investigation of the developed formulation in HCC-induced animal models, which will be reported separately upon completion.

5 Conclusion

We have developed novel PF127/CA/LEN@pMNCs by a coprecipitation method with sustained release profile beneficial for the treatment of HCC. PF127/CA/LEN@pMNCs exhibited a spherical morphology, homogeneous size distribution, and optimal charge, signifying that there was no development of agglomerates or physicochemical destabilization. The metallodrug demonstrated high drug loading capacity, sustained release, biocompatibility, increased Ms, and notable dispersibility. The PF127/CA/LEN@pMNCs were observed to be potential candidates for MH applications, thereby attaining necessary heating efficiencies at a low dose. Moreover, a significant antitumor potential of PF127/CA/LEN@pMNCs in H22 and Hep3B cells was established, more specifically when exposed to the MH conditions. Furthermore, an enhanced cytotoxic potential of the optimized PF127/CA/LEN@pMNCs was confirmed by LDH analysis. Besides this, no hemolytic potential of the formulation was observed. Overall, this study concluded that these multilayered multifunctional PF127/CA/LEN@pMNCs have excellent potential towards the treatment of HCC and could be employed for the management of other tumors as well.

Author contributions

Saba Sohail: data curation, investigation, writing first draft. Alam Zeb: methodology, investigation. Ali H. Alamri: software, resources. Adel Al Fatease: formal analysis, software. Ahmed A. Lahiq: wiring first draft, validation. Nabil K. Alruwaili: investigation, visualization. Salman Khan: formal analysis, visualization. Fakhar ud Din: conceptualization; resources, supervision, funding.

Data availability

Data will be available upon request.

Conflicts of interest

The author(s) confirm that they do not have any contradictory financial interests or personal relations that may have possibly influenced the results presented in this paper.

Acknowledgements

The authors express gratitude to the HEC for providing financial support for this research through its (NRPU project No: 20-14604/NRPU/R&D/HEC/2021) and Indigenous PhD Scholarship (Phase II), batch VI (PIN No. 520-143882-2MD6-12). The authors express their gratitude to the Higher Education Commission of Pakistan (HEC), Hanyang University in Ansan, South Korea, and the Department of Pharmacy of Quaid-i-Azam University in Islamabad, Pakistan, for their assistance in carrying out this study. Additionally, the authors are thankful to the Deanship of Scientific Research at King Khalid University for funding this work through a large group Research Project under grant number RGP2/441/45.

References

1 A. Villanueva, *N. Engl. J. Med.*, 2019, **380**, 1450–1462.
2 T. Yoshida, M. Kaibori, N. Fujisawa, M. Ishizuka, F. Sumiyama, M. Hatta, H. Kosaka, K. Matsui, K. Suzuki, T. O. Akama, T. Katano, K. Yoshii, M. Ebara and M. Sekimoto, *Nanomaterials*, 2022, **12**, 1364.
3 Y. Zhao, Y.-N. Zhang, K.-T. Wang and L. Chen, *Biochim. Biophys. Acta, Rev. Cancer*, 2020, **1874**, 188391.
4 J. Zong, H. Peng, X. Qing, Z. Fan, W. Xu, X. Du, R. Shi and Y. Zhang, *ACS Omega*, 2021, **6**, 12331–12342.

5 Y. Shi, J. Liu, Y. Zhang, J. Bao, J. Cheng and C. Yi, *Chin. Chem. Lett.*, 2021, **32**, 3189–3194.
6 Y. Sun, Y. Han, Y. Dou, X. Gong, H. Wang, X. Yu, Q. Wang, Y. Wang, Y. Dai, F. Ye, W. Jin and H. Zhang, *Bioact. Mater.*, 2022, **14**, 120–133.
7 L. Fu, W. Zhang, X. Zhou, J. Fu and C. He, *Bioact. Mater.*, 2022, **17**, 221–233.
8 A. Nair, K. Reece, M. B. Donoghue, W. V. Yuan, L. Rodriguez, P. Keegan and R. Pazdur, *Oncologist*, 2021, **26**, e484–e491.
9 M. Matsuki, T. Hoshi, Y. Yamamoto, M. Ikemori-Kawada, Y. Minoshima, Y. Funahashi and J. Matsui, *Cancer Med.*, 2018, **7**, 2641–2653.
10 X. Luo, S. Ao, C. Li, L. Fang, L. Chen, H. Liu, J. Li, Y. Zhou, X. Yin and C. Wu, *J. Drug Delivery Sci. Technol.*, 2023, **86**, 104631.
11 Y. Wu, R. Zhu, M. Zhou, J. Liu, K. Dong, S. Zhao, J. Cao, W. Wang, C. Sun, S. Wu, F. Wang, Y. Shi and Y. Sun, *Cancer Lett.*, 2023, **558**, 216106.
12 C. Fan, X. Zhu, Q. Zhou and W. Wang, *J. Oncol.*, 2022, **2022**, 2674163.
13 C. M. Chong, Z. Zhong, C. T. Vong, S. Wang, J. J. Lu, H. J. Zhong, H. Su and Y. Wang, *Curr. Neuropharmacol.*, 2021, **19**, 1090–1100.
14 D. Gao, Y. Shi, J. Ni, S. Chen, Y. Wang, B. Zhao, M. Song, X. Guo, X. Ren, X. Zhang, Z. Tian and Z. Yang, *Small*, 2022, **18**, e2106000.
15 F. U. Din, W. Aman, I. Ullah, O. S. Qureshi, O. Mustapha, S. Shafique and A. Zeb, *Int. J. Nanomed.*, 2017, **12**, 7291–7309.
16 M. J. Jeon, A. C. Gordon, A. C. Larson, J. W. Chung, Y. I. Kim and D. H. Kim, *Biomaterials*, 2016, **88**, 25–33.
17 A. Farzin, S. A. Etesami, J. Quint, A. Memic and A. Tamayol, *Adv. Healthcare Mater.*, 2020, **9**, e1901058.
18 S. Shatooti, M. Mozaffari, G. Reiter, D. Zahn and S. Dutz, *Sci. Rep.*, 2021, **11**, 16795.
19 K. Hayashi, M. Nakamura, H. Miki, S. Ozaki, M. Abe, T. Matsumoto, W. Sakamoto, T. Yogo and K. Ishimura, *Theranostics*, 2014, **4**, 834.
20 M. K. Lima-Tenório, E. A. G. Pineda, N. M. Ahmad, G. Agusti, S. Manzoor, D. Kabbaj, H. Fessi and A. Elaissari, *Colloids Surf., B*, 2016, **145**, 373–381.
21 S. Dutz and R. Hergt, *Nanotechnology*, 2014, **25**, 452001.
22 M. Malik, Z. Ali, S. Khan, A. Zeb, F. U. Din, A. H. Alamri and A. A. Lahiq, *J. Drug Delivery Sci. Technol.*, 2024, **91**, 105238.
23 F. U. Din, J. Y. Choi, D. W. Kim, O. Mustapha, D. S. Kim, R. K. Thapa, S. K. Ku, Y. S. Youn, K. T. Oh, C. S. Yong, J. O. Kim and H. G. Choi, *Drug Delivery*, 2017, **24**, 502–510.
24 F. U. Din, D. W. Kim, J. Y. Choi, R. K. Thapa, O. Mustapha, D. S. Kim, Y. K. Oh, S. K. Ku, Y. S. Youn, K. T. Oh, C. S. Yong, J. O. Kim and H. G. Choi, *Acta Biomater.*, 2017, **54**, 239–248.
25 Y. Cui, Y. Li, L. Fan, J. An, X. Wang, R. Fu and Z. Dong, *J. Pharm. Biomed. Anal.*, 2021, **206**, 114360.
26 H. Waqar, R. Riaz, N. M. Ahmed, A. I. Majeed and S. R. Abbas, *RSC Adv.*, 2022, **12**, 10504–10513.
27 M. W. Khan, C. Zou, S. Hassan, F. U. Din, M. Y. Abdoul Razak, A. Nawaz, Z. Alam, A. Wahab and S. A. Bangash, *RSC Adv.*, 2022, **12**, 14808–14818.
28 F. U. Din, S. G. Jin and H. G. Choi, *Polymers*, 2021, **13**(4), 551–561.
29 F. U. Din, J. S. Kim, H. C. Lee, S. Cheon, M. R. Woo, S. Woo, S. K. Ku, H. H. Yoo, J. O. Kim, S. G. Jin and H.-G. Choi, *J. Controlled Release*, 2024, **374**, 590–605.
30 H. Jamshaid, F. u Din, M. Malik, M. Mukhtiar, H. G. Choi, T. Ur-Rehman and G. M. Khan, *Sci. Rep.*, 2022, **12**, 14244.
31 H. Khalid, S. Batool, F. U. Din, S. Khan and G. M. Khan, *R. Soc. Open Sci.*, 2022, **9**, 220428.
32 S. Batool, F. Zahid, F. Ud-Din, S. S. Naz, M. J. Dar, M. W. Khan, A. Zeb and G. M. Khan, *Drug Dev. Ind. Pharm.*, 2021, **47**, 440–453.
33 M. I. Asad, D. Khan, A. U. Rehman, A. Elaissari and N. Ahmed, *Nanomaterials*, 2021, **11**, 3433.
34 A. Maryiam, S. Batool, Z. Ali, F. Zahid, A. H. Alamri, T. Alqahtani, A. A. Fatease, A. A. Lahiq, M. W. Khan and F. U. Din, *Pharm. Dev. Technol.*, 2025, **30**(1), 37–56.
35 S. Khizar, N. M. Ahmad, N. Ahmed, S. Manzoor, M. A. Hamayun, N. Naseer, M. K. L. Tenório, N. Lebaz and A. Elaissari, *Nanomaterials*, 2020, **10**, 2182.
36 M. Li, G. Fang, F. Zahid, R. Saleem, G. Ishrat, Z. Ali, M. Naeem and F. U. Din, *Heliyon*, 2024, **10**, e30290.
37 R. Riaz, H. Waqar, N. M. Ahmad and S. R. Abbas, *Polymers*, 2022, **14**, 2915.
38 A. A. Alghamdi, A. F. Alshahrani, N. H. Khdary, F. A. Alharthi, H. A. Alattas and S. F. Adil, *Materials*, 2018, **11**, 578.
39 J. Varshosaz, F. Hassanzadeh, H. S. Aliabadi, F. R. Khoraskani, M. Mirian and B. Behdadfar, *Int. J. Biol. Macromol.*, 2016, **93**, 1192–1205.
40 A. Anjum, K. Shabbir, F. U. Din, S. Shafique, S. S. Zaidi, A. H. Almari, T. Alqahtani, A. Maryiam, M. Moneeb Khan, A. Al Fatease, S. Bashir and G. M. Khan, *Drug Delivery*, 2023, **30**, 2173335.
41 Y. Wu, R. Zhu, M. Zhou, J. Liu, K. Dong, S. Zhao, J. Cao, W. Wang, C. Sun, S. Wu, F. Wang, Y. Shi and Y. Sun, *Cancer Lett.*, 2023, **558**, 216106.
42 X. Liu, Y. Huangfu, J. Wang, P. Kong, W. Tian, P. Liu, C. Fang, S. Li, Y. Nie, Z. Feng, P. Huang, S. Shi, C. Zhang, A. Dong and W. Wang, *Adv. Sci.*, 2023, **10**, e2300637.
43 Q. Wang, X. Zhu, X. Meng and H. Zhong, *Acta Biomater.*, 2023, **172**, 382–394.
44 Y. Zhang, M. Huo, J. Zhou, A. Zou, W. Li, C. Yao and S. Xie, *AAPS J.*, 2010, **12**, 263–271.
45 S. Maqsood, F. U. Din, S. U. Khan, E. Elahi, Z. Ali, H. Jamshaid, A. Zeb, T. Nadeem, W. Ahmed, S. Khan and H. G. Choi, *Life Sci.*, 2022, **311**, 121198.
46 A. Saleem, F. U. Din, Z. Ali, F. Zahid, A. Almari, A. Lahiq, T. Alqahtani and H. Alharbi, *J. Drug Delivery Sci. Technol.*, 2023, **91**, 105239.
47 S. Zhang, L. Zhao, X. Peng, Q. Sun, X. Liao, N. Gan, G. Zhao and H. Li, *Colloids Surf., B*, 2021, **201**, 111644.
48 K. Shahzad, S. Mushtaq, M. Rizwan, W. Khalid, M. Atif, F. U. Din, N. Ahmad, R. Abbasi and Z. Ali, *Mater. Sci. Eng.: C*, 2021, **119**, 111444.

49 Q. Wu, X. Chen, P. Wang, Q. Wu, X. Qi, X. Han, L. Chen, X. Meng and K. Xu, *ACS Appl. Mater. Interfaces*, 2020, **12**, 8016–8029.
50 J. Hu, Y. Dong, L. Ding, Y. Dong, Z. Wu, W. Wang, M. Shen and Y. Duan, *Signal Transduction Targeted Ther.*, 2019, **4**, 28.
51 B. W. Neun and M. A. Dobrovolskaia, *Characterization of Nanoparticles Intended for Drug Delivery*, 2011, pp. 215–224.
52 M. H. Al Nasir, S. Siddique, S. O. Aisida, Y. Altowairqi, M. M. Fadhali, M. Shariq, M. S. Khan, M. A. Qamar, T. Shahid, M. I. Shahzad and S. K. Ali, *Coatings*, 2022, **12**, 1272.
53 A. Bhardwaj, K. Parekh and N. Jain, *Sci. Rep.*, 2020, **10**, 15249.
54 M. Abul Kalam, A. A. Khan, S. Khan, A. Almalik and A. Alshamsan, *Int. J. Biol. Macromol.*, 2016, **87**, 329–340.
55 C.-L. Lin, C.-F. Lee and W.-Y. Chiu, *J. Colloid Interface Sci.*, 2005, **291**, 411–420.
56 J.-J. Lin, J.-S. Chen, S.-J. Huang, J.-H. Ko, Y.-M. Wang, T.-L. Chen and L.-F. Wang, *Biomaterials*, 2009, **30**, 5114–5124.
57 S. Khan, Z. H. Shah, S. Riaz, N. Ahmad, S. Islam, M. A. Raza and S. Naseem, *Ceram. Int.*, 2020, **46**, 10942–10951.
58 T. T. Hoang Thi, D.-H. Nguyen Tran, L. G. Bach, H. Vu-Quang, D. C. Nguyen, K. D. Park and D. H. Nguyen, *Pharmaceutics*, 2019, **11**, 120.
59 M. Hong, S. Li, W. Ji, M.-H. Qi and G.-B. Ren, *Cryst. Growth Des.*, 2021, **21**, 3714–3727.
60 V. Alfredo Reyes Villegas, J. Isaías De León Ramírez, E. Hernandez Guevara, S. Perez Sicairos, L. Angelica Hurtado Ayala and B. Landeros Sanchez, *J. Saudi Chem. Soc.*, 2020, **24**, 223–235.
61 M. Mostafa, O. Saleh, A. M. Henaish, S. A. Abd El-Kareem, R. Ghazy, O. M. Hemeda, A. M. Dorgham, H. Al-Ghamdi, A. H. Almuqrin, M. I. Sayyed, S. V. Trukhanov, E. L. Trukhanova, A. V. Trukhanov, D. Zhou and M. A. Darwish, *Nanomaterials*, 2022, **12**, 1045.
62 W. Fang, L. Yang, Y. Chen and Q. Hu, *Acta Biomater.*, 2023, **161**, 50–66.
63 R. Ma, Y. Wang, H. Qi, C. Shi, G. Wei, L. Xiao, Z. Huang, S. Liu, H. Yu, C. Teng, H. Liu, V. Murugadoss, J. Zhang, Y. Wang and Z. Guo, *Composites, Part B*, 2019, **167**, 396–405.
64 K. Vamvakidis, N. Maniotis and C. Dendrinou-Samara, *Nanoscale*, 2021, **13**, 6426–6438.
65 H. Wang, W. Bo, X. Feng, J. Zhang, G. Li and Y. Chen, *Int. J. Nanomed.*, 2024, **19**, 5581–5603.
66 A. F. Carneiro, C. N. Carneiro, L. de, N. Pires, L. S. Teixeira, S. M. Azcarate and F. de S Dias, *Talanta*, 2020, **219**, 121218.
67 Z. A. Özbek and P. G. Ergönül, *Food Hydrocolloids*, 2020, **107**, 105909.
68 J. R. Shin, G. S. An and S.-C. Choi, *Processes*, 2021, **9**, 1795.
69 N. Nagai, T. Isaka, S. Deguchi, M. Minami, M. Yamaguchi, H. Otake, N. Okamoto and Y. Nakazawa, *Int. J. Mol. Sci.*, 2020, **21**, 7083.
70 M. J. Jeon, A. C. Gordon, A. C. Larson, J. W. Chung, Y. I. Kim and D.-H. Kim, *Biomaterials*, 2016, **88**, 25–33.
71 W. K. Delan, M. Zakaria, B. Elsaadany, A. N. ElMeshad, W. Mamdouh and A. R. Fares, *Int. J. Pharm.*, 2020, **577**, 119038.
72 P. Haghighi, S. Ghaffari, S. Arbabi Bidgoli, M. Qomi and S. Haghighat, *Nanomed. Res. J.*, 2018, **3**, 71–78.
73 W. Y. Liu, C. C. Lin, Y. S. Hsieh and Y. T. Wu, *Molecules*, 2021, **26**, 3031.
74 G. Wang, X. Li, Y. Ma, Y. He, J. Hou, H. Che, X. Zhang, S. Han, Z. Wang, Z. Li and D. Li, *Ceram. Int.*, 2023, **49**, 32962–32970.
75 Z. Chaudhary, S. Subramaniam, G. M. Khan, M. M. Abeer, Z. Qu, T. Janjua, T. Kumeria, J. Batra and A. Popat, *Front. Bioeng. Biotechnol.*, 2019, **7**, 225.
76 H. Guo, X. Li, D. Mao, H. Wang, L. Wei, D. Qu, X. Qin, X. Li, Y. Liu and Y. Chen, *J. Nanobiotechnol.*, 2024, **22**, 206.
77 M. C. Mascolo, Y. Pei and T. Ring, *Materials*, 2013, **6**(12), 5549–5567.
78 H. Keshavarz, A. Khavandi, S. Alamolhoda and M. R. Naimi-Jamal, *RSC Adv.*, 2020, **10**, 39008–39016.
79 R. Hegazy, D. Rathod, A. Saraswat, R. Vartak, A. Muth and K. Patel, *J. Mol. Liq.*, 2024, **398**, 124263.
80 S. Nigam, K. Barick and D. Bahadur, *J. Magn. Mater.*, 2011, **323**, 237–243.
81 M. S. A. Darwish, L. M. Al-Harbi and A. Bakry, *J. Therm. Anal. Calorim.*, 2022, **147**, 11921–11930.
82 M. Nadeem, M. Ahmad, M. S. Akhtar, A. Shaari, S. Riaz, S. Naseem, M. Masood and M. A. Saeed, *PLoS One*, 2016, **11**, e0158084.
83 Z. Özcan and A. B. Hazar Yoruç, *Beilstein J. Nanotechnol.*, 2024, **15**, 256–269.
84 M. Abbasian, L. Razavi, M. Jaymand and S. Ghasemi Karaj-Abad, *Sci. Iran.*, 2019, **26**, 1447–1456.
85 G. B. Heggannavar, C. G. Hiremath, D. D. Achari, V. G. Pangarkar and M. Y. Kariduraganavar, *ACS Omega*, 2018, **3**, 8017–8026.
86 Wahajuddin and S. Arora, *Int. J. Nanomed.*, 2012, **7**, 3445–3471.
87 Y. Luo, J. Wang, L. Xu, Q. Du, N. Fang, H. Wu, F. Liu, L. Hu, J. Xu, J. Hou, Y. Zhong, Y. Liu, Z. Wang, H. Ran and D. Guo, *Acta Biomater.*, 2022, **154**, 478–496.
88 S. Batool, S. Sohail, F. ud Din, A. H. Alamri, A. S. Alqahtani, M. A. Alshahrani, M. A. Alshehri and H. G. Choi, *Drug Delivery*, 2023, **30**, 2183815.
89 M. J. Carrera Espinoza, K.-S. Lin, M.-T. Weng, S. C. Kunene, Y.-S. Lin and C.-M. Wu, *Pharmaceutics*, 2023, **15**, 740.
90 U. Shafique, F. u Din, S. Sohail, S. Batool, A. H. Almari, A. A. Lahiq, A. A. Fatease and H. M. Alharbi, *Int. J. Pharm.*, 2023, **646**, 123480.
91 S. Imtiaz, S. Sohail, F. U. Din, Z. Ali, S. Batool, M. Malik, A. Nawaz, A. H. Alamri, A. A. Lahiq, S. T. Alsharif and A. Asiri, *Pharm. Dev. Technol.*, 2024, **29**(7), 703–718.
92 N. Saleh, N. Ahmed, M. Imran Asad, I. Chaudhery and N. Mahmoud Ahmad, *IET Nanobiotechnol.*, 2020, **14**, 33–39.
93 J. Crezee, N. A. Franken and A. L. Oei, *Cancers*, 2021, **13**, 1240.
94 F. Reyes-Ortega, Á. V. Delgado, E. K. Schneider, B. Checa Fernández and G. Iglesias, *Polymers*, 2017, **10**, 10.
95 J. B. Mamani, J. P. Borges, A. M. Rossi and L. F. Gamarra, *Pharmaceutics*, 2023, **15**, 1663.

96 T. Miyazaki, T. Tange, M. Kawashita and B. Jeyadevan, *RSC Adv.*, 2020, **10**, 26374–26380.
97 M. Lázaro, P. Lupiáñez, J. L. Arias, M. P. Carrasco-Jiménez, Á. V. Delgado and G. R. Iglesias, *Polymers*, 2022, **14**, 4913.
98 P.-E. Le Renard, R. Lortz, C. Senatore, J.-P. Rapin, F. Buchegger, A. Petri-Fink, H. Hofmann, E. Doelker and O. Jordan, *J. Magn. Magn. Mater.*, 2011, **323**, 1054–1063.
99 N. Liu, A. Pyatakov, M. Zharkov, N. Pyataev, G. Sukhorukov, I. Alekhina, N. Perov, Y. Gun'ko and A. Tishin, *Appl. Phys. Lett.*, 2022, **120**, 102403.
100 F. Shubitidze, K. Kekalo, R. Stigliano and I. Baker, *J. Appl. Phys.*, 2015, **117**, 094302.
101 Q. A. Pankhurst, J. Connolly, S. K. Jones and J. Dobson, *J. Phys. D: Appl. Phys.*, 2003, **36**, R167.
102 Y. Itoh, Y. Yamada, Y. Kazaoka, T. Ishiguchi and N. Honda, *Exp. Ther. Med.*, 2010, **1**, 319–323.
103 K. Kameda, T. Kondo, K. Tanabe, Q. L. Zhao and H. Seto, *Int. J. Radiat. Oncol., Biol., Phys.*, 2001, **49**, 1369–1379.
104 J. Palzer, B. Mues, R. Goerg, M. Aberle, S. S. Rensen, S. W. M. Olde Damink, R. D. W. Vaes, T. Cramer, T. Schmitz-Rode, U. P. Neumann, I. Slabu and A. A. Roeth, *Int. J. Nanomed.*, 2021, **16**, 2965–2981.
105 C. Vergallo and L. Dini, *Sustainability*, 2018, **10**, 2776.